Journal of Nuclear Materials 393 (2009) 267–281

Contents lists available at ScienceDirect

Journal of Nuclear Materials

journal homepage: www.elsevier.com/locate/jnucmat

Thermodynamic investigations of ThO_2–UO_2 solid solutions

Smruti Dash *, S.C. Parida, Ziley Singh, B.K. Sen, V. Venugopal

Product Development Division, Bhabha Atomic Research Centre, Trombay, Mumbai 400 085, India

ARTICLE INFO

Article history:
Received 18 March 2009
Accepted 15 June 2009

ABSTRACT

Heat capacities and enthalpy increments of solid solutions $Th_{1-y}U_yO_2(s)$ (y = 0.0196, 0.0392, 0.0588, 0.098, 0.1964) and Simfuel (y = 0.0196) were measured by using a differential scanning calorimeter and a high temperature drop calorimeter. The heat capacities were measured in two temperature ranges: 127–305 K and 305–845 K and enthalpy increments were determined in the temperature range 891–1698 K. A heat capacity expression as a function of uranium content y and temperature and a set of self-consistent thermodynamic functions for $Th_{1-y}U_yO_2(s)$ were computed from present work and the literature data. The oxygen potentials of $Th_{1-y}U_yO_{2+x}(s)$ have been calculated and expressed as a polynomial functions of uranium content y, excess oxygen x and temperature T. The phase diagram, oxygen potential diagram of thorium–uranium–oxygen system and major vapour species over urania thoria mixed oxide have been computed using FactSage code.

1. Introduction

The Indian nuclear energy programme aims at large scale utilization of thorium for the sustained production of electricity in the country because of its limited uranium and vast thorium reserves [1,2]. India has a very ambitious power programme to utilize its thorium reserves in the Advanced Heavy Water Reactor (AHWR) [3,4]. The advantage of thoria based fuels is that fissile ^{233}U produced is burnt in the same reactor and the fissile content of the reactor increases with the time. The driver fuel of AHWR will be in the form ThO_2–2–3 wt% UO_2 and ThO_2–3–4 wt% PuO_2 solid solutions. To predict the performance of thoria based fuel or to generate a computer code for predicting in pile fuel behaviour, knowledge of thermophysical and thermodynamic properties such that heat capacity, thermal conductivity and thermal expansion, oxygen potential and vaporization behaviour of fuel material database is utmost important. The temperature of nuclear fuel is controlled by its specific heat capacity as well as thermal conductivity. Heat capacity can also be used for the calculation of thermal conductivity from thermal diffusivity. The oxygen potential of an oxide fuel material plays a key role in determining the mechanism of fuel clad chemical interaction. For any change in the oxygen potential close to stoichiometry, has a significant effect on the value of x in the mixed oxide $Th_{1-y}U_yO_{2+x}(s)$ fuel. It is therefore important to know the oxygen potential of the stoichiometric oxide. The knowledge of vaporization behaviour of fuel material gives information about various mass transport phenomenons in the fuel. The literature survey [5–29] on ThO_2–UO_2 system shows that enthalpy increments data [6–11], heat capacity [10], oxygen potential data [12–21], vaporization behaviour [22–24], thermal conductivity [25–28], thermal expansion [28,29] of thoria–urania mixed oxide solid solutions exist over a limited composition and temperature ranges. However, direct experimental heat capacity measurements for thoria rich (less than 10 mol% of urania) and oxygen potential measurements on stoichiometric mixed oxides $Th_{1-y}U_yO_2(s)$ have not been reported. In this study, heat capacity, enthalpy increments of $Th_{1-y}U_yO_2(s)$ (y = 0.0196, 0.0392, 0.0588, 0.098, 0.1964) have been determined using DSC-131 and Multi HTC 96, supplied by SETARAM Instrumentation, France. Studies on $Th_{1-y}U_yO_2(s)$ (y = 0.0196, 0.0392, 0.0588, 0.098, 0.1964) have been taken up considering higher use of $^{233}UO_2$ in the future thoria based fuels. The specific heat capacity was also measured for 4 at.% burn up $Th_{0.9804}U_{0.0196}O_2$ Simfuel. The phase diagram, oxygen potential diagram and major vapour species over mixed oxide have been computed using FactSage code [30]. A set of self-consistent thermodynamic functions for $Th_{1-y}U_yO_2(s)$ (y = 0.0196, 0.0392, 0.0588, 0.098, 0.1964) has been computed from the present work and that from experimental data reported in the literature.

2. Experimental

2.1. Material preparation

$Th_{1-y}U_yO_2(s)$ containing 0.0196, 0.0392, 0.0588, 0.098, 0.1964 mole% of $UO_2(s)$ were prepared by mixing 2, 4, 6, 10 and 20 wt% of $UO_2(s)$, respectively, with $ThO_2(s)$ and co-milled. $ThO_2(s)$ (total impurity < 1000 ppm) and $UO_2(s)$ (total impurity < 400 ppm) were used for mixed oxide preparation. Progressive milling technique was used for better homogeneity. The milled powers were

* Corresponding author. Tel.: +91 22 2559 0648; fax: +91 22 2550 5151.
E-mail address: smruti@barc.gov.in (S. Dash).

0022-3115/$ - see front matter © 2009 Published by Elsevier B.V.
doi:10.1016/j.jnucmat.2009.06.013

compacted at 300 MPa. The green pellets were sintered at 1923 K for 4 h in a molybdenum resistance furnace under flowing $N_2(g) + 8\%H_2(g)$. X-ray diffraction patterns of the materials thus prepared indicated homogeneous ThO_2–UO_2 solid solutions. For preparation of 4 at.% burn up Simfuel ($y = 0.0196$), computed amount of oxides of Ba, Sr, Ce, Zr, Mo, Ru, Y, La and Nd were added to required UO_2–ThO_2 mixed oxide.

2.2. Differential scanning calorimeter

Heat capacity measurements were carried out using a heat flux type differential scanning calorimeter, DSC-131 supplied by SETARAM Instrumentation, France. In this technique, the change of the difference in the heat flow rate to the sample and an inert reference material is measured. The sample and reference crucibles are positioned symmetrically to the centre on a plate shaped DSC-131 transducer. Transducer and DSC crucibles are enclosed in a small cylindrical silver furnace which dissipates heat to the crucibles. When the furnace is heated, heat flows through the DSC transducer to the crucibles, in an ideal situation same amount of heat flows into the sample and reference crucibles. A differential signal is generated due to different heat flux to sample and reference. This differential temperature signal is proportional to the heat flow rate measured in the form of electrical potential difference that is calibrated using NIST reference materials. The temperature and heat calibrations were carried out using phase transition temperatures and transition heats of same NIST reference materials [31].

2.3. Heat capacity measurements

The detailed experimental procedure adopted has been described earlier [31]. In DSC-131, heat capacities of $Th_{1-y}U_yO_2(s)$ ($y = 0$, 0.0196, 0.0392, 0.0588, 0.098, 0.1964) and Simfuel were measured in two different modes (i) continuous (low temperature) and (ii) step mode (high temperature). In the continuous mode, temperature was increased continuously from 126 K to 305 K. However, in the step mode, the whole temperature range from room temperature to 863 K was divided into 14 equal intervals with steps of 40 K. Stability time of 600 s was given in each step up to maximum temperature. In both the methods, the molar heat capacities were measured with identical experimental conditions in the three runs. In the first run, two empty identical aluminum crucibles of identical masses and 10^{-4} dm^3 capacity with covering lid were kept in the sample and reference cells and the heat flow versus temperature were recorded. In the second run, the heat flow versus temperature were recorded by loading NIST synthetic sapphire (SRM-720) in the powder form (~200 mg) into the aluminum crucible in the sample cell keeping the crucible in the reference cell empty. In the third run, heat flow versus temperature were measured by loading the actual experimental sample (~200 mg) in the powder form into the aluminum crucible in the sample side and keeping the crucible in the reference side empty. In all the three sets of experiments, high purity argon as a carrier gas with the flow rate of 3 dm^3 h^{-1} and furnace heating rate of 5 K min^{-1} were maintained. Helium was used as carrier gas for low temperature heat capacity measurements. At least three runs were carried out for each sample at each temperature.

2.4. Multi-detector high temperature calorimeter

The heat contents corresponding to the enthalpy increments from ambient temperature to the respective temperature of a given run were determined using SETARAM multi-detector high temperature calorimeter (MHTC-96) operating in drop mode. The tubular calorimeter consists of a working chamber with volume 5.3 cm^3 with the inserted Pt-crucible and an empty reference chamber positioned vertically below. Twenty-eight thermocouples covering the whole surface and providing an integrated heat exchange at the output signal. Platinum crucible is centered in a gas-tight $Al_2O_3(s)$ tube placed in the furnace heated by a graphite resistance element. All measurements were performed in flowing high purity argon. The sample and reference materials are arranged alternatively in the feeding chamber and equilibrated at ambient temperature that is measured prior to each drop. In the meantime, the detector is maintained at a given temperature and the samples are dropped from the feeding chamber into the working chamber of the sensor. Sufficient time was given for stabilization of both the temperature and heat flux. The heat flux ϕ in volts is monitored as a function of time τ in seconds and the peak area $\int \phi d\tau$ (after subtracting a base line ϕ_B) associated with each drop corresponds to the respective enthalpy increments. From the reference material drops, the actual instrument sensitivity can be determined as:

$$S = \frac{\int (\phi_R - \phi_B) d\tau}{\int_{T_a}^{T_m} C^o_{P,R} dT} \cdot \frac{M_R}{m_R} \tag{1}$$

where ϕ_R, ϕ_B, T_a and T_m are measured heat flux of the reference and blank and the ambient and measurement temperature, respectively, the latter being evaluated as an average from the values taken in a steady state before and after the drop, m_R and M_R are the reference material mass and molar mass, respectively, $C^\circ_{p,R}$ stands for molar heat capacity of the reference material. The enthalpy increment corresponding to heating the sample material from T_a to T_m is given by

$$H^\circ_m(T) - H^\circ_m\ (298.15\ \mathrm{K}) = \int \frac{(\phi_s - \varphi_B) d\tau \cdot M_S}{S \cdot m_s} \tag{2}$$

where ϕ_s is the measured heat flux of the sample.

2.5. Measurement of enthalpy increments

The calorimeter was calibrated by dropping samples of synthetic sapphire (SRM 720) suppli1ed by NIST, USA. In a typical experiment at a given temperature, mixed oxide solid solutions and $Al_2O_3(s)$, maintained at the ambient temperature were dropped, alternatively, into the calorimeter maintained at required temperature.

3. Results

3.1. Heat capacity using DSC

The heat capacities of pure $ThO_2(s)$ are measured in the temperature range 318–836 K and are given in Table 1, which includes a comparison to the literature values [32]. The heat capacities of $Th_{1-y}U_yO_2(s)$ and Simfuel are determined in two different temperature ranges: (i) 126–305 K and (ii) 304–846 K and are given in Tables 2–7. These tables also include a comparison of computed heat capacity vales of $\{1 - y(ThO_2(s)) + yUO_2(s)\}$ [32]. The errors in the heat capacity measurements are within 3% [31].

3.2. Low temperature heat capacity

The heat capacity values for $Th_{1-y}U_yO_2$ and Simfuel ($y = 0.0196$), given in Tables 2–7, are best least-squares fitted into the following expressions:

$Th_{0.9804}U_{0.0196}O_2(s)$

$$\begin{aligned} C^\circ_{p,m}\ (\mathrm{J\,K^{-1}\,mol^{-1}}) = {} & -460.08 + 2.9205 \cdot (T/\mathrm{K}) - 6.09 \times 10^{-3} \cdot (T/\mathrm{K})^2 \\ & + 4.367 \times 10^{-6}\ (T/\mathrm{K})^3 + 9.349 \times 10^6 \cdot (\mathrm{K}/T)^2 \\ & - 7.566 \times 10^8 \cdot (\mathrm{K}/T)^3 \quad (127 \le T/\mathrm{K} \le 304), \end{aligned} \tag{3}$$

Table 1
Enthalpy increment and heat capacity data for ThO_2(s).

High temperature heat capacity data		$H^\circ_m(T) - H^\circ_m(298.15\ K)$ data		Comparisons of heat capacity data			
T/K	$C^\circ_{p,m}(T)$/J K^{-1} mol^{-1}	T/K	ΔH^T_{298} (J mol^{-1}) Exp	T/K	$C^\circ_{p,m}(T)$/J K^{-1} mol^{-1} Fit^{*cp}	$C^\circ_{p,m}(T)$/J K^{-1} mol^{-1} Ref. [30]	$\Delta C^\circ_{p,m}(T)$/J K^{-1} mol^{-1}
318.4	62.65	891.7	42 417	300	61.07	61.92	−0.8
357.4	65.31	941.6	46 317	400	67.17	67.69	−0.5
396.9	67.12	1041.5	54 084	500	70.41	70.74	−0.3
436.9	68.30	1141.1	61 933	600	72.53	72.74	−0.2
476.7	69.70	1191.6	65 952	700	74.11	74.24	−0.1
516.4	70.80	1241.4	69 938	800	75.40	75.48	−0.1
556.2	71.71	1341.1	77 995	900	76.53	76.59	−0.1
596.0	72.47	1390.7	82 037	1000	77.56	77.61	0.0
635.9	73.13	1491.4	90 317	1100	78.53	78.58	−0.1
675.8	73.70	1539.4	94 294	1200	79.44	79.53	−0.1
715.8	74.22	1589.1	98 449	1300	80.33	80.45	−0.1
755.8	74.69	1639.4	102 508	1400	81.19	81.37	−0.2
795.8	75.12	1690.2	106 719	1500	82.03	82.29	−0.3
835.9	75.52			1600	82.86	83.21	−0.3
				1700	83.68	84.14	−0.5

$\Delta H^T_{298} = H^\circ_m(T) - H^\circ_m(298.15\ K)$, *cp = combined fit of heat capacity data obtained in this study (Table 8), $\Delta C^\circ_{p,m}(T) = C^\circ_{p,m}(Th_{1-y}U_yO_2, s, T) - \{(1-y)C^\circ_{p,m}(ThO_2, s, T) + yC^\circ_{p,m}(UO_2, s, T)\}$.

Table 2
Heat capacity and enthalpy increment data for $Th_{0.9804}U_{0.0196}O_2$(s).

Low temperature heat capacity data				High temperature heat capacity data		$H^\circ_m(T) - H^\circ_m(298.15\ K)$ data		Comparisons of heat capacity data			
T/K	$C^\circ_{p,m}(T)$/ J K^{-1} mol^{-1}	T/K	$C^\circ_{p,m}(T)$ (J K^{-1} mol^{-1})	T/K	$C^\circ_{p,m}(T)$ (J K^{-1} mol^{-1})	T/K	ΔH^T_{298} Exp (J mol^{-1})	T/K	$C^\circ_{p,m}(T)$ (J K^{-1} mol^{-1}) Fit^{*cp}	$C^\circ_{p,m}(T)$ (J K^{-1} mol^{-1}) Ref. [30]	$\Delta C^\circ_{p,m}(T)$ (J K^{-1} mol^{-1})
127.0	32.14	243.6	58.35	303.6	62.06	890.9	42 572	300	61.69	61.96	−0.3
134.2	38.37	253.5	58.91	318.3	63.15	940.8	46 640	400	67.82	67.80	0.0
141.7	43.49	258.5	59.66	357.3	65.06	990.2	50 240	500	71.02	70.87	0.1
149.2	47.48	264.5	60.04	396.8	67.60	1039.9	54 333	600	73.06	72.86	0.2
156.7	49.36	272.2	60.78	436.8	69.58	1089.9	57 999	700	74.55	74.35	0.2
164.3	50.48	280.0	61.23	476.6	70.94	1139.8	62 131	800	75.76	75.59	0.2
171.8	51.23	287.8	61.43	516.2	71.62	1189.3	65 819	900	76.79	76.69	0.1
177.0	52.36	295.6	61.84	556.1	72.55	1239.1	69 975	1000	77.73	77.71	0.0
184.4	53.11	303.6	62.06	595.9	73.35	1288.7	73 740	1100	78.59	78.68	−0.1
194.8	53.85			635.8	73.97	1389.3	82 200	1200	79.40	79.64	−0.2
202.5	54.78			675.7	74.34	1488.5	89 999	1300	80.19	80.58	−0.4
208.9	55.72			715.7	74.78	1588.2	98 370	1400	80.95	81.52	−0.6
216.4	56.66			755.7	75.06	1688.0	106 636	1500	81.69	82.46	−0.8
225.6	56.85			795.7	75.27			1600	82.42	83.41	−1.0
233.4	57.6			835.8	75.64			1700	83.14	84.38	−1.2

$\Delta H^T_{298} = H^\circ_m(T) - H^\circ_m(298.15\ K$, *cp = combined fit of heat capacity data obtained in this study (Table 8), $\Delta C^\circ_{p,m}(T) = C^\circ_{p,m}(Th_{1-y}U_yO_2, s, T) - \{(1-y)C^\circ_{p,m}(ThO_2, s, T) + yC^\circ_{p,m}(UO_2, s, T)\}$.

Table 3
Heat capacity and enthalpy increment data for $Th_{0.9608}U_{0.0392}O_2$(s).

Low temperature heat capacity data				High temperature heat capacity data				$H^\circ_m(T) - H^\circ_m(298.15\ K)$ data		Comparisons of heat capacity data			
T/K	$C^\circ_{p,m}(T)$ (J K^{-1} mol^{-1})	T/K	$C^\circ_{p,m}(T)$ (J K^{-1} mol^{-1})	T/K	$C^\circ_{p,m}(T)$ (J K^{-1} mol^{-1})	T/K	$C^\circ_{p,m}(T)$ (J K^{-1} mol^{-1})	T/K	ΔH^T_{298} Exp/J mol^{-1}	T/K	$C^\circ_{p,m}(T)$ (J K^{-1} mol^{-1}) Fit^{*cp}	$C^\circ_{p,m}(T)$ (J K^{-1} mol^{-1} Ref.[30]	$\Delta C^\circ_{p,m}(T)$ (J K^{-1} mol^{-1})
126.8	32.58	217.7	55.92	305.0	59.41	584.4	71.22	900.5	42756	300	59.41	61.99	−2.6
132.5	37.93	223.9	56.52	307.4	60.23	604.5	71.28	951.0	46674	400	65.78	67.91	−2.1
138.5	41.79	230.1	56.52	326.7	61.83	624.4	71.78	1001.1	50385	500	69.08	71.00	−1.9
144.5	44.81	236.4	57.12	346.1	63.15	644.5	71.94	1039.9	53369	600	71.16	72.99	−1.8
150.4	47.10	242.6	57.36	365.6	64.23	664.5	72.27	1089.9	57209	700	72.68	74.47	−1.8
156.4	49.27	248.8	57.60	385.2	64.97	684.5	72.40	1100.9	58057	800	73.90	75.70	−1.8
162.5	50.12	255.0	57.72	404.9	65.84	704.6	72.52	1150.8	61910	900	74.94	76.79	−1.9
168.5	51.08	261.3	58.09	424.8	66.52	724.6	72.77	1239.1	68768	1000	75.87	77.81	−1.9
174.6	52.18	267.5	58.21	444.8	67.57	744.7	72.98	1288.7	72641	1100	76.72	78.79	−2.1
180.8	53.02	273.7	58.57	464.8	68.06	764.8	73.17	1389.3	80541	1200	77.53	79.75	−2.2
186.9	53.62	280	58.69	484.7	68.93	784.9	73.55	1488.5	88387	1300	78.30	80.70	−2.4
193.0	54.35	286.2	59.05	504.6	69.55	805	73.74	1597.4	97063	1400	79.05	81.66	−2.6
199.2	54.83	292.5	59.05	524.5	69.67	825.1	73.93	1697.7	105211	1500	79.78	82.63	−2.8
205.4	55.31	298.7	59.41	544.5	70.24	845.3	74.31			1600	80.50	83.62	−3.1
211.5	55.67	305	59.41	564.5	70.53					1700	81.20	84.62	−3.4

$\Delta H^T_{298} = H^\circ_m(T) - H^\circ_m(298.15\ K)$, ^{*cp} = combined fit of heat capacity data obtained in this study (Table 8), $\Delta C^\circ_{p,m}(T) = C^\circ_{p,m}(Th_{1-y}U_yO_2, s, T) - \{(1-y)C^\circ_{p,m}(ThO_2, s, T) + yC^\circ_{p,m}(UO_2, s, T)\}$.

Table 4
Heat capacity data for $Th_{0.9412}U_{0.0588}O_2(s)$ as a function of temperature.

Low temperature heat capacity data				High temperature heat capacity data				Comparisons of heat capacity data			
T/K	$C^\circ_{p,m}(T)$/ J K^{-1} mol^{-1}	T/K	$C^\circ_{p,m}(T)$/ J K^{-1} mol^{-1}	T/K	$C^\circ_{p,m}(T)$/ J K^{-1} mol^{-1}	T/K	$C^\circ_{p,m}(T)$/ J K^{-1} mol^{-1}	T/K	$C^\circ_{p,m}(T)$/ J K^{-1} mol^{-1} Fit^{*cp}	$C^\circ_{p,m}(T)$/ J K^{-1} mol^{-1} Ref. [30]	$\Delta C^\circ_{p,m}(T)$/ J K^{-1} mol^{-1}
127.0	32.22	217.8	51.89	305.1	59.87	584.4	69.70	300	59.25	62.03	−2.8
132.7	34.92	224.0	52.76	307.4	59.62	604.4	70.07	350	62.83	65.60	−2.8
138.7	37.06	230.2	53.32	326.7	61.50	624.4	70.46	400	65.23	68.03	−2.8
144.7	38.76	236.4	53.89	346.1	62.61	644.4	70.75	450	66.95	69.78	−2.8
150.6	40.27	242.6	54.43	365.6	63.57	664.5	71.08	500	68.25	71.13	−2.8
156.6	41.79	248.8	55.03	385.2	64.49	684.5	71.13	550	69.26	72.21	−2.9
162.7	43.11	255.1	55.78	405.0	65.47	704.6	71.46	600	70.09	73.11	−2.9
168.7	44.26	261.3	56.16	424.9	66.24	724.7	71.61	650	70.78	73.89	−3.0
174.8	45.23	267.5	56.85	444.9	66.79	744.8	71.85	700	71.38	74.59	−3.1
180.9	46.52	273.8	57.29	464.8	67.45	764.9	72.04	750	71.90	75.22	−3.2
187.0	47.78	280.0	57.67	484.7	67.95	785.0	72.24	800	72.37	75.81	−3.3
193.1	48.78	286.2	58.18	504.7	68.43	805.2	72.45	850	72.80	76.36	−3.4
199.3	49.73	292.5	58.49	524.6	68.72	825.3	72.62	900	73.19	76.89	−3.6
205.4	50.29	298.8	59.15	544.5	69.15	845.5	72.73				
211.6	51.24	305.1	59.64	564.5	69.49						

$\Delta H^T_{298} = H^\circ_m(T) - H^\circ_m(298.15\ K)$, ^{*cp}= combined fit of heat capacity data obtained in this study (Table 8), $\Delta C^\circ_{p,m}(T) = C^\circ_{p,m}(Th_{1-y}U_yO_2, s, T) - \{(1-y)C^\circ_{p,m}(ThO_2, s, T) + yC^\circ_{p,m}(UO_2, s, T)\}$.

Table 5
Heat capacity and enthalpy increment data for $Th_{0.902}U_{0.098}O_2(s)$.

Low temperature heat capacity data				High temperature heat capacity data		$H^\circ_m(T) - H^\circ_m(298.15\ K)$ data		Comparisons of heat capacity data			
T/K	$C^\circ_{p,m}(T)$/ J K^{-1} mol^{-1}	T/K	$C^\circ_{p,m}(T)$/ J K^{-1} mol^{-1}	T/K	$C^\circ_{p,m}(T)$/ J K^{-1} mol^{-1}	T/K	ΔH^T_{298} Exp/ J mol^{-1}	T/K	$C^\circ_{p,m}(T)$/ J K^{-1} mol^{-1} Fit^{*cp}	$C^\circ_{p,m}(T)$/J K^{-1} mol^{-1} Ref. [30]	$\Delta C^\circ_{p,m}(T)$/ J K^{-1} mol^{-1}
126.8	32.69	241.1	57.49	303.4	61.66	890.7	42572	300	61.46	62.11	−0.7
134.0	35.89	248.9	58.27	318.4	61.99	940.8	46690	400	67.69	68.25	−0.6
141.6	38.69	256.7	59.06	357.3	65.75	990.8	50331	500	71.00	71.38	−0.4
149.1	40.86	264.5	59.56	396.8	68.14	1040.6	54463	600	73.18	73.36	−0.2
156.6	42.66	272.2	60.10	436.8	69.75	1090.5	58130	700	74.81	74.82	0.0
164.2	44.20	280.0	60.42	476.7	70.88	1140.6	62340	800	76.16	76.02	0.1
171.7	46.19	287.8	61.03	516.3	71.76	1190.2	66043	900	77.33	77.10	0.2
179.4	47.72	295.6	61.41	556.1	72.51	1239.3	70238	1000	78.41	78.11	0.3
187.0	48.97	303.4	61.66	595.9	73.19	1289.8	74077	1100	79.41	79.09	0.3
194.7	50.40			635.8	73.86	1338.7	78312	1200	80.37	80.08	0.3
202.4	51.77			675.7	74.53	1387.9	82078	1300	81.30	81.08	0.2
210.1	53.07			715.7	75.22	1488.7	90888	1400	82.20	82.09	0.1
217.9	54.29			755.7	75.8	1537.8	94749	1500	83.08	83.14	−0.1
225.6	55.4			795.7	76.01	1638.8	103584	1600	83.96	84.22	−0.3
233.4	56.39			835.7	76.27	1688.8	107815	1700	84.82	85.34	−0.5

$\Delta H^T_{298} = H^\circ_m(T) - H^\circ_m(298.15\ K)$, ^{*cp} = combined fit of heat capacity data obtained in this study (Table 8), $\Delta C^\circ_{p,m}(T) = C^\circ_{p,m}(Th_{1-y}U_yO_2, s, T) - \{(1-y)C^\circ_{p,m}(ThO_2, s, T) + yC^\circ_{p,m}(UO_2, s, T)\}$.

Table 6
Heat capacity and enthalpy increment data for $Th_{0.8036}U_{0.1964}O_2(s)$.

Low temperature heat capacity data				High temperature heat capacity data		$H^\circ_m(T) - H^\circ_m(298.15\ K)$ data		Comparison of heat capacity data			
T/K	$C^\circ_{p,m}(T)$/ J K^{-1} mol^{-1}	T/K	$C^\circ_{p,m}(T)$/ J K^{-1} mol^{-1}	T/K	$C^\circ_{p,m}(T)$/ J K^{-1} mol^{-1}	T/K	ΔH^T_{298} Exp/ J mol^{-1}	T/K	$C^\circ_{p,m}(T)$/ J K^{-1} mol^{-1} Fit ^{*cp}	$C^\circ_{p,m}(T)$/J K^{-1} mol^{-1} Ref. [30]	$\Delta C^\circ_{p,m}(T)$/ J K^{-1} mol^{-1}
127.0	33.23	241.2	58.10	303.5	62.41	891.9	42799	300	62.25	62.30	−0.1
134.2	36.89	249.0	58.91	318.5	62.93	941.7	47020	400	68.55	68.82	−0.3
141.7	39.95	256.7	59.18	357.4	66.08	991.8	50709	500	71.90	72.03	−0.1
149.2	42.03	264.5	59.90	396.9	68.84	1041.3	54899	600	74.09	73.99	0.1
156.7	44.56	272.3	60.22	436.9	70.79	1091.8	58688	700	75.73	75.41	0.3
164.3	46.19	280.1	60.81	476.7	72.11	1141.3	62813	800	77.08	76.56	0.5
171.8	48.02	287.9	61.26	516.4	73.0	1240.9	70404	900	78.26	77.61	0.6
179.5	50.08	295.7	61.79	556.2	73.61	1291.1	74675	1000	79.33	78.61	0.7
187.1	51.88	303.5	62.16	596.1	74.41	1340.4	78532	1100	80.33	79.61	0.7
194.8	52.80			635.9	75.02	1390.8	82805	1200	81.29	80.64	0.7
202.5	54.03			675.8	75.46	1440.0	86781	1300	82.21	81.70	0.5
210.2	54.85			715.8	75.83	1490.1	91051	1400	83.11	82.82	0.3
217.9	55.87			755.8	76.26	1589.9	99304	1500	83.99	84.00	0.0
225.7	56.67			795.8	76.65	1640.1	103651	1600	84.86	85.24	−0.4
233.4	57.64			835.9	77.13	1690	108001	1700	85.72	86.54	−0.8

$\Delta H^T_{298} = H^\circ_m(T) - H^\circ_m(298.15\ K)$, ^{*cp} = combined fit of heat capacity data obtained in this study (Table 8), $\Delta C^\circ_{p,m}(T) = C^\circ_{p,m}(Th_{1-y}U_yO_2, s, T) - \{(1-y)C^\circ_{p,m}(ThO_2, s, T) + yC^\circ_{p,m}(UO_2, s, T)\}$.

Table 7
Heat capacity data for Simfuel (4 at.% burn up thoria-urania ($Th_{0.9804}U_{0.0196}O_2$).

Low temperature heat capacity data				High temperature heat capacity data			
T/K	$C^\circ_{p,m}(T)$/J K^{-1} mol^{-1}	T/K	$C^\circ_{p,m}(T)$/J K^{-1} mol^{-1}	T/K	$C^\circ_{p,m}(T)$/J K^{-1} mol^{-1})	T/K	$C^\circ_{p,m}(T)$/J K^{-1} mol^{-1}
126.9	0.126	217.8	0.213	307.3	0.235	824.3	0.29
134.1	0.144	225.6	0.216	326.8	0.241	844.5	0.29
141.6	0.162	233.3	0.219	346.2	0.245		
149.1	0.175	241.1	0.221	365.7	0.249		
156.6	0.185	248.9	0.222	405.1	0.256		
164.2	0.191	256.6	0.223	464.7	0.267		
171.8	0.195	264.4	0.224	484.6	0.269		
179.4	0.199	272.2	0.224	584.1	0.277		
187.0	0.202	280.0	0.224	604.1	0.278		
194.7	0.204	287.8	0.225	703.9	0.286		
202.4	0.207	295.5	0.226	723.9	0.286		
210.1	0.21	303.3	0.227	804.1	0.289		

$\Delta H^T_{298} = H^\circ_m(T) - H^\circ_m(298.15\ K)$, ^{*cp} = combined fit of heat capacity data obtained in this study (Table 8).

$Th_{0.9608}U_{0.0392}O_2(s)$

$$C^\circ_{p,m}(J\,K^{-1}\,mol^{-1}) = -445.92 + 3.2945\cdot(T/K) - 8.51\times10^{-3}\cdot(T/K)^2 + 8.115\times10^{-6}\cdot(T/K)^3 + 7.769\times10^{6}\cdot(K/T)^2 - 6.16\times10^{8}\cdot(K/T)^3 \quad (127 \le T/K \le 305) \tag{4}$$

$Th_{0.9412}U_{0.0588}O_2(s)$

$$C^\circ_{p,m}(J\,K^{-1}\,mol^{-1}) = -372.82 + 3.1827\cdot(T/K) - 9.10\times10^{-3}\cdot(T/K)^2 + 9.545\times10^{-6}\cdot(T/K)^3 + 4.448\times10^{6}\cdot(K/T)^2 - 3.025\times10^{8}\cdot(K/T) \quad (127 \le T/K \le 305), \tag{5}$$

$Th_{0.902}U_{0.098}O_2(s)$

$$C^\circ_{p,m}(J\,K^{-1}\,mol^{-1}) = -499.91 + 3.8795\cdot(T/K) - 1.015\times10^{-2}\cdot(T/K)^2 + 9.478\times10^{-6}\cdot(T/K)^3 + 6.388\times10^{6}\cdot(K/T)^2 - 4.34\times10^{8}\cdot(K/T) \quad (127 \le T/K \le 303), \tag{6}$$

$Th_{0.8036}U_{0.1964}O_2(s)$

$$C^\circ_{p,m}(J\,K^{-1}\,mol^{-1}) = -310.22 + 2.9556\cdot(T/K) - 8.98\times10^{-3}\cdot(T/K)^2 + 9.847\times10^{-6}\cdot(T/K)^3 + 3.196\times10^{6}\cdot(K/T)^2 - 2.158\times10^{8}\cdot(K/T)^3 \quad (127 \le T/K \le 304), \tag{7}$$

Simfuel

$$C^\circ_{p,m}(J\,K^{-1}\,g^{-1}) = -0.6743 + 4.450\times10^{-3}\cdot(T/K) - 6.791\times10^{-6}\cdot(T/K)^2 + 1.274\times10^{-9}\cdot(T/K)^3 + 1.824\times10^{4}\cdot(K/T)^2 - 1.617\times10^{6}\cdot(K/T)^3 \quad (127 \le T/K \le 303). \tag{8}$$

The $C^\circ_{p,m}(298.15\ K)$ values for $Th_{0.9804}U_{0.0196}O_2(s)$, $Th_{0.9608}U_{0.0392}O_2(s)$, $Th_{0.9412}U_{0.0588}O_2(s)$, $Th_{0.902}U_{0.098}O_2(s)$ and $Th_{0.8036}U_{0.1964}O_2(s)$ have been calculated from Eqs. (3)–(7) as 61.68, 59.08, 58.77, 61.18 and 61.52 J K^{-1} mol^{-1}, respectively.

3.3. High temperature heat capacity

The heat capacities of ThO_2, $Th_{1-y}U_yO_2(s)$, and Simfuel are least-squares fitted as a function of temperature. The corresponding expressions are:

$ThO_2(s)$

$$C^\circ_{p,m}(J\,K^{-1}\,mol^{-1}) = 71.25 + 7.10\times10^{-3}\cdot(T/K) - 10.998\times10^{5}\cdot(K/T)^2 \quad (318 \le T/K \le 836), \tag{9}$$

$Th_{0.9804}U_{0.0196}O_2(s)$

$$C^\circ_{p,m}(J\,K^{-1}\,mol^{-1}) = 74.92 + 3.26\times10^{-3}\cdot(T/K) - 13.118\times10^{5}\cdot(K/T)^2 \quad (304 \le T/K \le 836), \tag{10}$$

$Th_{0.9608}U_{0.0392}O_2(s)$

$$C^\circ_{p,m}(J\,K^{-1}\,mol^{-1}) = 71.72 + 4.920\times10^{-3}\cdot(T/K) - 12.525\times10^{5}\cdot(K/T)^2 \quad (305 \le T/K \le 845), \tag{11}$$

$Th_{0.9412}U_{0.0588}O_2(s)$

$$C^\circ_{p,m}(J\,K^{-1}\,mol^{-1}) = 70.56 + 4.49\times10^{-3}\cdot(T/K) - 11.395\times10^{5}\cdot(K/T)^2 \quad (305 \le T/K \le 846), \tag{12}$$

$Th_{0.902}U_{0.098}O_2(s)$

$$C^\circ_{p,m}(J\,K^{-1}\,mol^{-1}) = 74.79 + 4.15\times10^{-3}\cdot(T/K) - 13.586\times10^{5}\cdot(K/T)^2 \quad (303 \le T/K \le 836), \tag{13}$$

$Th_{0.8036}U_{0.1964}O_2(s)$

$$C^\circ_{p,m}(J\,K^{-1}\,mol^{-1}) = 77.52 + 1.88\times10^{-3}\cdot(T/K) - 14.930\times10^{5}\cdot(K/T)^2 \quad (304 \le T/K \le 836), \tag{14}$$

Simfuel

$$C^\circ_{p,m}(J\,K^{-1}\,g^{-1}) = 0.27554 + 3.0\times10^{-5}\cdot(T/K) - 4.668\times10^{3}\cdot(K/T)^2 \quad (307 \le T/K \le 845). \tag{15}$$

3.4. Enthalpy increments

The experimentally determined enthalpy increment data acquired by multi-HTC are listed in Tables 1–3, 5 and 6. Enthalpy increment values of each solid solution were least-squares fitted into polynomial equation using Shomate method [33] with constraints, (i) $H^\circ_m(T) - H^\circ_m(298.15\ K) = 0$ at 298.15 K and (ii) $C^\circ_{p,m}(298.15\ K) =$ known value. $C^\circ_{p,m}(298.15\ K)$ values have been taken from our low temperature ($127 \leqslant T/K \leqslant 305$ K) DSC data. The following sets of polynomial equations were obtained.

$ThO_2(s)$

$$H^\circ_m(T) - H^\circ_m\ (298.15\ K)\ (J\,mol^{-1}) = 69.95\cdot(T/K) + 4.393\times10^{-3}\cdot(T/K)^2 + 9.61\times10^{5}\cdot(K/T) - 24470 \quad (892 \le T/K \le 1690) \tag{16}$$

$Th_{0.9804}U_{0.0196}O_2(s)$

$$H^\circ_m(T) - H^\circ_m\ (298.15\ K)\ (J\,mol^{-1}) = 71.87\cdot(T/K) + 3.524\times10^{-3}\cdot(T/K)^2 + 10.923\times10^{5}\cdot(K/T) - 25404 \quad (891 \le T/K \le 1688) \tag{17}$$

$Th_{0.9608}U_{0.0392}O_2(s)$

$$H^\circ_m(T) - H^\circ_m\ (298.15\ K)\ (J\,mol^{-1}) = 73.77\cdot(T/K) + 2.063\times10^{-3}\cdot(T/K)^2 + 14.154\times10^{5}\cdot(K/T) - 26926 \quad (901 \le T/K \le 1698), \tag{18}$$

$Th_{0.902}U_{0.098}O_2(s)$

$$H^\circ_m(T) - H^\circ_m\ (298.15\ K)\ (J\ mol^{-1}) = 70.69\cdot(T/K) + 4.454\times10^{-3}\cdot(T/K)^2 + 10.81\times10^5\cdot(K/T) - 25096 \quad (891 \le T/K \le 1689), \qquad (19)$$

$Th_{0.8036}U_{0.1964}O_2(s)$

$$H^\circ_m(T) - H^\circ_m\ (298.15\ K)\ (J\ mol^{-1}) = 72.23\cdot(T/K) + 3.769\times10^{-3}\cdot(T/K)^2 + 11.521\times10^5\cdot(K/T) - 25736 \quad (892 \le T/K \le 1690). \qquad (20)$$

The heat capacity expression of $ThO_2(s)$ and thoria–urania solid solutions were obtained by differentiating enthalpy increment expressions (16)-(20) with respect to temperature and are given in Table 8. The heat capacity data obtained from DSC and Multi HTC were least-squares fitted into single combined polynomial expressions for $Th_{1-y}U_yO_2$ (y = 0.0196, 0.0392, 0.098, 0.1964) and are also given in Table 8.

3.5. Phase diagram

The chemical investigations on Th–U–O system is reported in the literature [34,35]. Paul and Keller [34] observed $U_2Th_2O_9(s)$ compound in Th–U–O system by solid state reaction. Boekschoten and Kema [35] have prepared $ThUO_5(s)$ by co-precipitation of mixtures of solutions of $Th(NO_3)_4(aq)$ and $UO_2(NO_3)_4(aq)$ with NaOH(aq) and heating the precipitates above 483 K. The authors [35] have studied X-ray diffraction pattern and thermal stability of this compound. JCPDS files [36] did not show $U_2Th_2O_9(s)$, however, $ThUO_5(s)$ [35] is reported. The present authors have prepared $UThO_5(s)$ by gel combustion technique. In this method, required stoichiometric amounts of $Th(NO_3)_4(aq)$ and $UO_2(NO_3)_4(aq)$ (Indian Rare Earth, India) solutions were mixed together and the resultant solution was mixed with aqueous citric acid solution under constant stirring condition and the total metal ions to citric acid ratio was kept constant as 1.5:1. The resulting solution was evaporated at 350 K under constant stirring condition and continuous evaporation lead to gel formation which was self-ignited, and an ignition front propagated through the whole mass, leaving a light black flaky powder which was heated at 450 K for 12 h under flowing oxygen at 1 bar pressure. It was then calcined at 850 K for 150 h in oxygen. The product was analyzed by XRD and found to match with JCPDS file number 22-0492 [36]. Hence, $ThUO_5(s)$ has been taken as the only ternary compound present in Th–U–O system for phase diagram calculations. The heat capacity and entropy at 298.15 K for $ThUO_5(s)$ have been calculated using additive oxide method and component oxide data were taken from the literature [32]. $\Delta_f H^\circ_m$ ($UThO_5$,s,298.15 K) has been estimated using methods given by Kubashewski et al. [37] and is calculated as $-2475.9\ kJ\ mol^{-1}$. Using required data, $\Delta_f G^\circ_m(UThO_5,s,T)$ has been calculated and is given as:

$$\Delta_f G^\circ_m(UThO_5, s, T)\ kJ\ mol^{-1} = -2475.9 + 0.4601\cdot(T/K). \qquad (21)$$

The Gibbs energy values of binary compounds from JANAF tables [32], $UThO_5(s)$ from Eq. (21) and the optimized experimental data for $Th_{1-y}U_yO_2$ reported in Tables 9–13 and from the literature [6–10], were used for the computation of the phase diagram of Th–U–O system. It has been calculated at 900 K and 101.325 kPa using FactSage code [30] and is shown in Fig. 1. It shows that $ThO_2(s)$ forms solid solutions with $UO_2(s)$ in the complete range of $UO_2(s)$ but $U_3O_8(s)$ does not dissolve any $ThO_2(s)$. $ThUO_5(s)$ which is stable up to 1070 K is present on the section between $UO_3(s)$ and $ThO_2(s)$.

3.6. Oxygen potential diagram

The oxygen potential diagram of Th–U–O_2 system at 900 K is shown in Fig. 2. The mixed oxide at a particular temperature is characterized by a definite partial pressure of gaseous oxygen which is in thermodynamic equilibrium with the solid. Fig. 2 depicts the stable phases at different partial pressures of oxygen in Th–U–O_2 system. The calculations show that $Th_{1-y}U_yO_2(s)$ solid solutions are stable in air even at 1500 K. $ThUO_5(s)$ phase precipitates at 900 K and $U_3O_8(s)$ phase at 1273 K from the $Th_{1-y}U_yO_2(s)$ solid solutions in air.

The oxygen potentials of $Th_{1-y}U_yO_2(s)$ (y = 0.0196, 0.0392, 0.0588, 0.098, 0.1964) have been calculated using FactSage code [30] and found to range from −440 to $-550\ kJ\ mol^{-1}$ at 1473 K. It was observed that the oxygen potential of mixed oxides decreases with increase in y value which could be due to decrease of mean uranium valence. The oxygen potentials of $Th_{1-y}U_yO_2(s)$ obtained in this study are more negative in the small O/M region near the stoichiometric compositions than the previous results by Tanaka et al. [15], Ugajin [16], Ugajin et al. [17], but are close to Matsui and Naito [18]. The oxygen potential measurements on stoichiometric oxides are required to check this value. The oxygen potential of $Th_{1-y}U_yO_{2+x}(s)$ has also been calculated from the literature [16,21].

3.7. Vapour pressure

The optimized experimental data reported in Tables 9–13 were used to compute the vaporization behaviour of $Th_{1-y}U_yO_2(s)$. Calculations showed the major gaseous species over $Th_{1-y}U_yO_2(s)$ is $UO_2(g)$ and over $Th_{1-y}U_yO_{2+x}(s)$ is $UO_3(g)$. The main gaseous species over $Th_{0.9804}U_{0.0196}O_2(s)$ are $UO_2(g)$, $UO_3(g)$, UO(g), $ThO_2(g)$, U(g), ThO(g), O(g) and $O_2(g)$. The calculated partial Gibbs energy of these species over $Th_{1-y}U_yO_2(s)$ solid solution as a function of U/(Th + U) fractions have been computed at 2300 K and is shown in Fig. 3. It is observed that the partial pressures of $UO_2(g)$ and $ThO_2(g)$ appear to be nearly independent of the U/(Th + U) fraction. It also shows that uranium-bearing species in the vapour phase is more than thorium-bearing species.

4. Discussion

4.1. Heat capacity

4.1.1. ThO_2–UO_2 solid solutions

The heat capacities of $ThO_2(s)$ obtained in this study are compared with that reported in the literature [20,32,38,39] in Fig. 4 which also compares $C^\circ_{p,m}(T)$ values of $UO_2(s)$ [32,38,40]. It shows that heat capacity values of $ThO_2(s)$ measured in this study match well with that of JANAF tables [32], ASTD [38] and Fischet et al. [39]. Similarly, heat capacity data of JANAF tables [32] and ASTD [38] match well for $UO_2(s)$. Hence for computation of heat capacities of $Th_{1-y}U_yO_2(s)$, $ThO_2(s)$ and $UO_2(s)$, data were taken from JANAF tables [32]. The heat capacity difference ($\Delta C^\circ_{p,m}(T)$) between experimentally measured $Th_{1-y}U_yO_2(s)$ and corresponding component oxides have been calculated for different U/(Th + U) fractions. These values are plotted against temperature in Fig. 5. Except, heat capacities of y = 0.0392 and 0.0588, rest other heat capacity values of $Th_{1-y}U_yO_2$ are bunched around zero deviation line, which represents same heat capacity values for $Th_{1-y}U_yO_2(s)$ and $\{1-y(ThO_2(s)) + yUO_2(s)\}$. The deviation is largest at y = 0.0588.

The calorimetric data reported in the literature [6–10] are summarized in Table 14. Springer et al. [6] have measured the heat capacity of the $ThO_2(s)$ and $UO_2(s)$ solid solution indirectly by drop calorimetry from 273 to 2271 K for samples containing 10.3 and

Table 8
Coefficients of the fit equations of enthalpy increment and heat capacity data of $Th_{1-y}U_yO_2(s)$ solid solutions, obtained in this study.

Authors/ years	Wt% $UO_2(s)$	Solid solutions	Temp range (K)	Method	$H^\circ_m(T) - H^\circ_m(298.15\ K)/J\ mol^{-1} = A \cdot (T/K) + B \cdot (T/K)^2 + C \cdot (K/T) + D$				$C^\circ_{p,m}(T)/J\ K^{-1}\ mol^{-1} = a + b \cdot (T/K) + d \cdot (K/T)^2 + e \cdot (T/K)^3 + c \cdot (K/T)^2 + f \cdot (K/T)^3$					
					A	$B \times 10^3$	$C \times 10^{-5}$	$-D$	a	b	$d \times 10^3$	$e \times 10^6$	$-c \times 10^{-6}$	$f \times 10^{-8}$
		$ThO_2(s)$	318–836	DSC	71.25	3.550	10.998	25 248	71.25	0.0071	–	–	1.0998	–
			892–1690	MHTC	69.95	4.393	9.610	24 470	69.95	0.008786	–	–	0.9610	–
			318–1690	CP	70.94	3.86	10.968	25 173	70.94	0.00772	–	–	1.0968	–
			324–2949	CL	69.58	4.566	9.371	24 294	69.58	.009132	–	–	0.9371	–
	2	$Th_{0.9804}U_{0.0196}O_2(s)$	127–304	DSC	–	–	–	–	−460.08	2.9205	−6.09	4.367	−9.349	−7.566
			304-836	DSC	74.92	1.630	13.118	26 882	74.92	0.00326	–	–	1.3118	–
			891–1688	MHTC	71.87	3.524	10.923	25 404	71.87	0.007048	–	–	1.0923	–
			304–1688	CP	72.17	3.34	11.234	25 582	72.17	0. 00668	–	–	1.1234	–
			304–1688	CL	73.46	2.965	13.056	26 545	73.46	0.00593	–	–	1.3056	
	4	$Th_{0.9608}U_{0.0392}O_2(s)$	127–305	DSC	–	–	–	-	−445.92	3.2945	−8.51	8.115	−7.769	−6.16
			305–845	DSC	71.72	2.46	12.525	25 803	71.72	0.00492	–	–	1.2525	–
			901–1698	MHTC	73.77	2.063	14.154	26 926	73.77	0.004126	–	–	1.4154	–
			308–1698	CP	70.51	3.265	11.750	25 254	70.51	0.00653	–	–	1.1750	–
			308–1698	CL	70.56	3.295	11.498	25 187	70.56	0.00659	–	–	1.1498	–
	6	$Th_{0.9412}U_{0.0588}O_2(s)$	127–305	DSC	–	–	–	–	−372.82	3.1827	−9.10	9.545	−4.448	−3.025
			305–846	DSC	70.56	2.245	11.395	25 059	70.56	0.00449	–	–	1.1395	–
			305–991	CL	72.41	4.55	12.760	25 909	72.41	0.00091	–	–	1.2760	–
	10	$Th_{0.902}U_{0.098}O_2(s)$	127–303	DSC	–	–	–	–	-499.91	3.8795	−1.015	9.478	−6.388	−4.34
			303–836	DSC	74.79	2.075	13.586	27 040	74.79	0.00415	–	–	1.3586	–
			891–1689	MHTC	70.69	4.454	10.810	25 096	70.69	0.008908	–	–	1.0810	–
			304–1688	CP	71.40	4.06	11.139	25 385	71.40	0.00812	–	–	1.1139	–
			304–2271	CL	71.74	3.495	10.092	25 085	71.74	0.00699	–	–	1.0092	–
	20	$Th_{0.8036}U_{0.1964}O_2(s)$	127–304	DSC	–	–	–	–	−310.22	2.9556	−8.98	9.847	−3.196	−2.158
			304–836	DSC	77.52	0.940	14.930	28 204	77.52	0.00188	–	–	1.4930	–
			892–1690	MHTC	72.23	3.769	11.521	25 736	72.23	0.007538	–	–	1.1521	–
			304–1690	CP	72.39	4.035	11.308	25 734	72.392	.00807	–	–	1.1308	–
			304–2270	CL	72.76	3.535	10.160	25 415	72.76	0.00707	–	–	1.0160	–

DSC, differential scanning calorimeter; MHTC, multi high temperature calorimeter; CP, combined fit of heat capacity data obtained in this study from DSC and MTHC; CL, combined fit of heat capacity data of literature and present study.

Table 9
Thermodynamic functions for $Th_{0.9804}U_{0.0196}O_2(s)$.

T/K	$C^\circ_{p,m}(T)$/ J K^{-1} mol^{-1}	$H^\circ_m(T) - H^\circ_m(298.15\ K)$/ kJ mol^{-1}	$S^\circ_m(T)$/ J K^{-1} mol^{-1}	$\phi^\circ_m(T)$/ J K^{-1} mol^{-1}	$H^\circ_m(T)$/ kJ mol^{-1}	$G^\circ_m(T)$/ kJ mol^{-1}	$\Delta_f H^\circ_m(T)$/ kJ mol^{-1}	$\Delta_f G^\circ_m(T)$/ kJ mol^{-1}
298.15	61.52	0.0	66.3	66.3	−1223.6	−1243.4	−1223.6	−1166.8
300	61.69	0.1	66.6	66.3	−1223.5	−1243.5	−1223.6	−1166.4
400	67.82	6.6	85.3	68.8	−1217.0	−1251.2	−1222.7	−1147.6
500	71.02	13.6	100.8	73.6	−1210.0	−1260.4	−1221.6	−1128.8
600	73.06	20.8	114.0	79.3	−1202.8	−1271.2	−1220.4	−1110.4
700	74.55	28.2	125.4	85.1	−1195.4	−1283.2	−1219.2	−1092.2
800	75.76	35.7	135.4	90.8	−1187.9	−1296.3	−1218.0	−1074.1
900	76.80	43.3	144.4	96.3	−1180.3	−1310.3	−1217.0	−1056.2
1000	77.73	51.1	152.5	101.4	−1172.5	−1325.0	−1215.9	−1038.2
1100	78.59	58.9	160.0	106.5	−1164.7	−1340.7	−1215.0	−1020.6
1200	79.41	66.8	166.9	111.2	−1156.8	−1357.1	−1214.0	−1003.0
1300	80.19	74.7	173.2	115.7	−1148.9	−1374.1	−1213.2	−985.4
1400	80.95	82.8	179.2	120.1	−1140.8	−1391.7	−1212.3	−967.9
1500	81.69	90.9	184.8	124.2	−1132.7	−1409.9	−1211.7	−950.5
1600	82.42	99.1	190.1	128.2	−1124.5	−1428.7	−1210.9	−933.2
1700	83.14	107.4	195.1	131.9	−1116.2	−1447.9	−1213.4	−915.7
1800	83.85	115.8	199.9	135.6	−1107.8	−1467.7	−1212.4	−898.2
1900	84.55	124.2	204.5	139.1	−1099.4	−1488.0	−1211.5	−880.9
2000	85.25	132.7	208.8	142.5	−1090.9	−1508.5	−1210.7	−863.3

Table 10
Thermodynamic functions for $Th_{0.9608}U_{0.0392}O_2(s)$.

T/K	$C^\circ_{p,m}(T)$/ J K^{-1} mol^{-1}	$H^\circ_m(T) - H^\circ_m(298.15\ K)$/ kJ mol^{-1}	$S^\circ_m(T)$/ J K^{-1} mol^{-1}	$\phi^\circ_m(T)$/ J K^{-1} mol^{-1}	$H^\circ_m(T)$/ kJ mol^{-1}	$G^\circ_m(T)$/ kJ mol^{-1}	$\Delta_f H^\circ_m(T)$/ kJ mol^{-1}	$\Delta_f G^\circ_m(T)$/ kJ mol^{-1}
298.15	59.55	0.0	67.1	67.1	−1220.9	−1240.9	−1220.9	−1164.3
300	59.72	0.1	67.4	67.1	−1220.8	−1241.0	−1220.9	−1164.0
400	65.95	6.4	85.6	69.6	−1214.5	−1248.7	−1220.3	−1145.1
500	69.19	13.2	100.7	74.3	−1207.7	−1258.0	−1219.3	−1126.4
600	71.24	20.2	113.5	79.8	−1200.7	−1268.8	−1218.3	−1108.0
700	72.73	27.4	124.6	85.5	−1193.5	−1280.7	−1217.3	−1089.7
800	73.92	34.8	134.4	90.9	−1186.1	−1293.6	−1216.3	−1071.4
900	74.95	42.2	143.1	96.2	−1178.7	−1307.5	−1215.4	−1053.4
1000	75.86	49.8	151.1	101.3	−1171.1	−1322.2	−1214.7	−1035.4
1100	76.70	57.4	158.4	106.2	−1163.5	−1337.7	−1214.1	−1017.6
1200	77.50	65.1	165.1	110.9	−1155.8	−1353.9	−1213.3	−999.7
1300	78.26	72.9	171.3	115.2	−1148.0	−1370.7	−1212.6	−982.0
1400	79.00	80.7	177.1	119.5	−1140.2	−1388.1	−1212.0	−964.2
1500	79.72	88.7	182.6	123.5	−1132.2	−1406.1	−1211.6	−946.5
1600	80.43	96.7	187.8	127.4	−1124.2	−1424.6	−1211.1	−928.9
1700	81.13	104.8	192.7	131.1	−1116.1	−1443.7	−1213.8	−911.2
1800	81.82	112.9	197.3	134.6	−1108.0	−1463.1	−1213.1	−893.3
1900	82.50	121.1	201.8	138.1	−1099.8	−1483.2	−1212.4	−875.7
2000	83.17	129.4	206.0	141.3	−1091.5	−1503.5	−1211.8	−857.9

Table 11
Thermodynamic functions for $Th_{0.9412}U_{0.0588}O_2(s)$.

T/K	$C^\circ_{p,m}(T)$/ J K^{-1} mol^{-1}	$H^\circ_m(T) - H^\circ_m(298.15\ K)$/ kJ mol^{-1}	$S^\circ_m(T)$/ J K^{-1} mol^{-1}	$\phi^\circ_m(T)$/ J K^{-1} mol^{-1}	$H^\circ_m(T)$/ kJ mol^{-1}	$G^\circ_m(T)$/ kJ mol^{-1}	$\Delta_f H^\circ_m(T)$/ kJ mol^{-1}	$\Delta_f G^\circ_m(T)$/ kJ mol^{-1}
298.15	59.08	0.0	67.8	67.8	−1218.1	−1238.3	−1218.1	−1161.7
300	59.25	0.1	68.1	67.8	−1218.0	−1238.4	−1218.1	−1161.4
400	65.23	6.4	86.1	70.1	−1211.7	−1246.1	−1217.5	−1142.5
500	68.25	13.1	101.0	74.8	−1205.0	−1255.5	−1216.6	−1123.9
600	70.09	20.0	113.7	80.4	−1198.1	−1266.3	−1215.7	−1105.5
700	71.38	27.1	124.6	85.9	−1191.0	−1278.2	−1214.8	−1087.2
800	72.37	34.3	134.2	91.3	−1183.8	−1291.2	−1214.0	−1069.0
900	73.19	41.5	142.7	96.6	−1176.6	−1305.0	−1213.4	−1050.9
1000	75.79	49.7	151.7	102.0	−1168.4	−1320.1	−1212.1	−1033.3
1100	76.59	57.3	159.0	106.9	−1160.8	−1335.7	−1211.6	−1015.5
1200	77.34	65.0	165.6	111.4	−1153.1	−1351.8	−1210.8	−997.6
1300	78.06	72.8	171.9	115.9	−1145.3	−1368.8	−1210.2	−980.0
1400	76.87	79.7	177.1	120.2	−1138.4	−1386.3	−1210.5	−962.3
1500	77.87	87.7	183.1	124.6	−1130.4	−1405.0	−1210.3	−945.3
1600	79.35	96.1	188.8	128.7	−1122.0	−1424.1	−1209.4	−928.2
1700	80.24	104.3	193.7	132.3	−1113.8	−1443.1	−1211.9	−910.4
1800	81.60	112.9	198.9	136.2	−1105.2	−1463.2	−1210.7	−893.1
1900	82.46	121.2	203.4	139.6	−1096.9	−1483.4	−1210.0	−875.6
2000	83.22	128.7	206.6	142.3	−1089.4	−1502.6	−1210.2	−856.7

Table 12
Thermodynamic functions for $Th_{0.902}U_{0.098}O_2(s)$.

T/K	$C^\circ_{p,m}(T)$/ J K^{-1} mol^{-1}	$H^\circ_m(T) - H^\circ_m(298.15\ K)$/ kJ mol^{-1}	$S^\circ_m(T)$/ J K^{-1} mol^{-1}	$\phi^\circ_m(T)$/ J K^{-1} mol^{-1}	$H^\circ_m(T)$/ kJ mol-1	$G^\circ_m(T)$/ kJ mol^{-1}	$\Delta_f H^\circ_m(T)$/ kJ mol^{-1}	$\Delta_f G^\circ_m(T)$/ kJ mol^{-1}
298.15	62.47	0.0	69.1	69.1	−1212.5	−1233.1	−1212.5	−1156.6
300	62.62	0.1	69.4	69.1	−1212.4	−1233.3	−1212.5	−1156.3
400	68.23	6.7	88.3	71.6	−1205.8	−1241.2	−1211.6	−1137.6
500	71.20	13.7	103.9	76.5	−1198.8	−1250.8	−1210.4	−1119.2
600	73.13	20.9	117.1	82.3	−1191.6	−1261.9	−1209.3	−1101.1
700	74.57	28.3	128.4	88.0	−1184.2	−1274.1	−1208.1	−1083.1
800	75.76	35.8	138.5	93.8	−1176.7	−1287.5	−1207.0	−1065.4
900	76.79	43.4	147.5	99.3	−1169.1	−1301.9	−1206.1	−1047.8
1000	77.72	51.2	155.6	104.4	−1161.3	−1316.9	−1205.3	−1030.1
1100	78.59	59.0	163.0	109.4	−1153.5	−1332.8	−1204.9	−1012.5
1200	79.43	66.9	169.9	114.2	−1145.6	−1349.5	−1203.9	−995.2
1300	80.23	74.9	176.3	118.7	−1137.6	−1366.8	−1203.0	−977.8
1400	81.01	82.9	182.3	123.1	−1129.6	−1384.9	−1202.2	−960.6
1500	81.78	91.1	187.9	127.2	−1121.4	−1403.3	−1202.3	−943.2
1600	82.53	99.3	193.2	131.1	−1113.2	−1422.4	−1201.6	−926.0
1700	83.27	107.6	198.2	134.9	−1104.9	−1441.9	−1203.9	−908.7
1800	84.01	115.9	203.0	138.6	−1096.6	−1462.0	−1203.1	−891.4
1900	84.74	124.4	207.6	142.1	−1088.1	−1482.6	−1202.2	−874.1
2000	85.47	132.9	211.9	145.5	−1079.6	−1503.4	−1201.4	−856.7

Table 13
Thermodynamic functions for $Th_{0.8036}U_{0.1964}O_2(s)$.

T/K	$C^\circ_{p,m}(T)$/ J K^{-1} mol^{-1}	$H^\circ_m(T) - H^\circ_m(298.15\ K)$/ kJ mol^{-1}	$S^\circ_m(T)$/ J K^{-1} mol^{-1}	$\phi^\circ_m(T)$/ J K^{-1} mol^{-1}	$H^\circ_m(T)$/ kJ mol-1	$G^\circ_m(T)$/ kJ mol^{-1}	$\Delta_f H^\circ_m(T)$/ kJ mol^{-1}	$\Delta_f G^\circ_m(T)$/ kJ mol^{-1}
298.15	63.44	0.0	71.7	71.7	−1198.6	−1220.0	−1198.6	−1143.5
300	63.59	0.1	72.1	71.8	−1198.5	−1220.2	−1198.6	−1143.2
400	69.24	6.8	91.2	74.2	−1191.8	−1228.3	−1197.6	−1124.8
500	72.23	13.9	107.0	79.2	−1184.7	−1238.2	−1196.4	−1106.7
600	74.18	21.2	120.4	85.1	−1177.4	−1249.7	−1195.2	−1089.0
700	75.64	28.7	131.9	90.9	−1169.9	−1262.3	−1194.0	−1071.4
800	76.83	36.3	142.1	96.7	−1162.3	−1276.0	−1192.9	−1053.9
900	77.87	44.1	151.2	102.2	−1154.5	−1290.6	−1191.9	−1036.5
1000	78.81	51.9	159.5	107.6	−1146.7	−1306.2	−1191.5	−1019.3
1100	79.70	59.8	167.0	112.6	−1138.8	−1322.5	−1191.5	−1002.1
1200	80.54	67.8	174.0	117.5	−1130.8	−1339.6	−1190.5	−984.9
1300	81.35	75.9	180.5	122.1	−1122.7	−1357.4	−1189.5	−967.9
1400	82.14	84.1	186.5	126.4	−1114.5	−1375.6	−1188.6	−950.7
1500	82.91	92.4	192.2	130.6	−1106.2	−1394.5	−1189.5	−933.6
1600	83.68	100.7	197.6	134.7	−1097.9	−1414.1	−1188.8	−916.7
1700	84.43	109.1	202.7	138.5	−1089.5	−1434.1	−1190.7	−899.6
1800	85.17	117.6	207.5	142.2	−1081.0	−1454.5	−1189.8	−882.4
1900	85.91	126.1	212.2	145.8	−1072.5	−1475.7	−1189.0	−865.6
2000	86.65	134.8	216.6	149.2	−1063.8	−1497.0	−1188.2	−848.4

20.4 wt% UO_2. They have given least squares fit expression for the enthalpy increment data using $H^\circ_m(T) - H^\circ_m(273\ K) = 0$. In order to compare data given by Springer et al. [6] with the literature, the enthalpy increment values of Springer et al. [6] were corrected by subtracting $H^\circ_m(298.15\ K) - H^\circ_m(273\ K)$ value, calculated from the polynomial fit. These corrected values were 1299 and 1145 J mol^{-1} for 10.3 and 20.4 wt% UO_2(s), respectively. For the sake of comparison, calculated enthalpy increments data of Springer et al. [6] is given in Table 14. Fischer et al. [6] have measured $H^\circ_m(T) - H^\circ_m(298.15\ K)$ for $Th_{0.08}U_{0.92}O_2(s)$, $Th_{0.15}U_{0.85}O_2(s)$ and $Th_{0.7}U_{0.3}O_2(s)$ in the temperature range 2300–3400 K using inverse drop calorimeter. The authors marked a discontinuity in the enthalpy increment data of these solid solutions. They reported these transition temperatures as 2850, 2900 and 2950 K for $Th_{0.08}U_{0.92}O_2(s)$, $Th_{0.15}U_{0.85}O_2(s)$ and $Th_{0.7}U_{0.3}O_2(s)$, respectively. Fink [41] analyzed enthalpy increment data of $UO_2(s)$, $ThO_2(s)$, $PuO_2(s)$, $Th_{1-y}U_yO_2(s)$ and $Pu_{1-y}O_2(s)$ to study complex behaviour of actinide oxide systems. Anthonysamy et al. [7] and Kandan et al. [9] have measured enthalpy increments of $Th_{1-y}U_yO_2(s)$ mixed oxide solid solutions with $y = 0.1$, 0.5 and 0.9 using drop calorimeter in the temperature range 473–973 K and 479–1805 K, respectively. Kandan et al. [10] have measured heat capacity in the temperature range 298.15–800 K for the same compositions of mixed oxide solid solutions using DSC. Agarwal et al. [9] have measured enthalpy increments of $ThO_2(s)$, $Th_{0.9804}U_{0.0196}O_2(s)$, $Th_{0.0961}U_{0.0392}O_2(s)$, $Th_{0.941}U_{0.0588}O_2(s)$, $Th_{0.902}U_{0.098}O_2(s)$ and Simfuel of $Th_{0.9804}U_{0.0196}O_2(s)$ using a high temperature Calvet calorimeter in the temperature range 375–991 K.

Figs. 6–10 show comparison of heat capacity values of overlapped composition of present study and that of the literature. The measured heat capacities of each ThO_2–UO_2 solid solution and its derived heat capacities data from enthalpy increments measured in this study are compared with the derived heat capacity data reported in the literature [6–9], pure thoria [32], pure urania [32] and computed $C^\circ_{p,m}(T)$ values from additive oxide data. Figs. 6–8 compare heat capacity data by Agarwal et al. [9], present study and data calculated from additive oxide method for $y = 0.0196$, 0.0392 and 0.0588, respectively. Except $y = 0.0588$ mole UO_2, former two mixed oxides show reasonably good agreement. The heat capacity data of $Th_{0.9412}U_{0.0588}O_2(s)$ by Agarwal et al. [9] are higher than that of present study and this difference increases with increase in temperature and it is about 4% higher at the

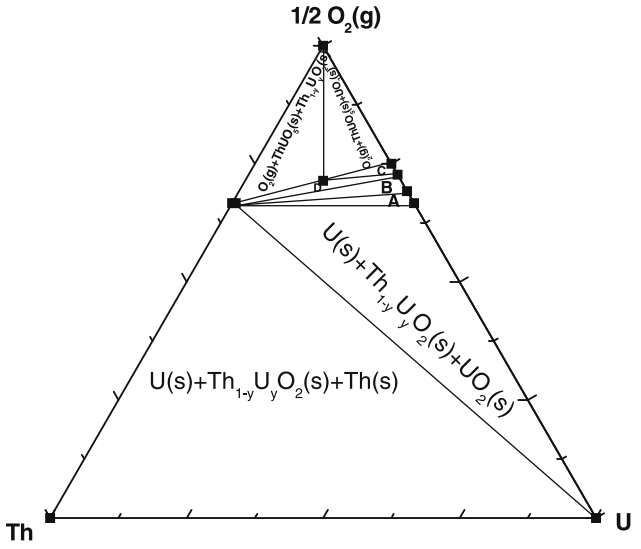

Fig. 1. Phase diagram for the system Th–U–O at 900 K. The equilibrium phase fields: A = $UO_2(s) + U_4O_9(s) + Th_{1-y}U_yO_2(s)$, B = $U_4O_9(s) + U_3O_8(s) + Th_{1-y}U_yO_2(s)$, C = $U_3O_8(s) + UO_3(s) + ThUO_5(s)$ and D = $U_3O_8(s) + Th_{1-y}U_yO_2(s) + ThUO_5(s)$. $Th_{1-y}U_yO_2(s)$ represents solid solutions of different U/(Th + U) fractions.

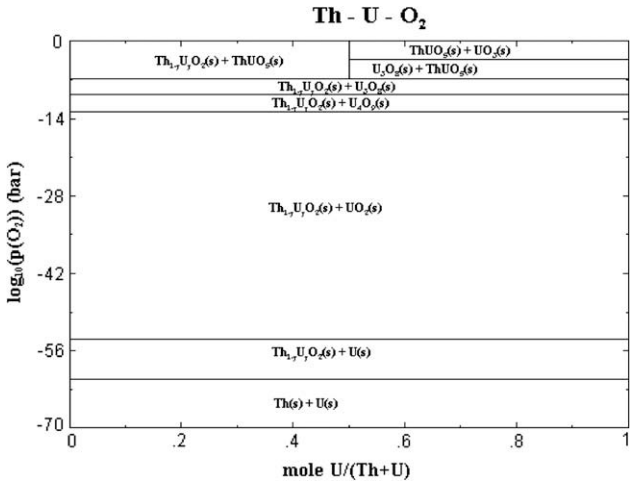

Fig. 2. Oxygen potential diagram for Th–U–O_2 system at 900 K.

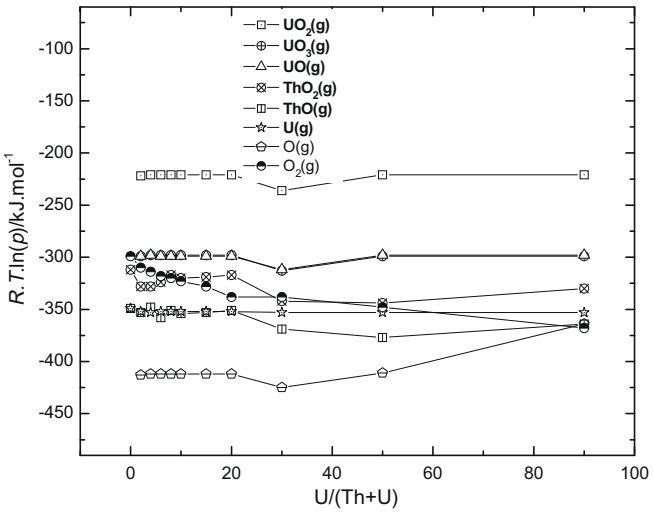

Fig. 3. The variation of partial molar Gibbs energy of $UO_2(g)$, $UO_3(g)$, UO(g), $ThO_2(g)$, ThO(g),O(g) and $O_2(g)$ with U/(Th + U) fraction in $Th_{1-y}U_yO_2(s)$ at 2300 K.

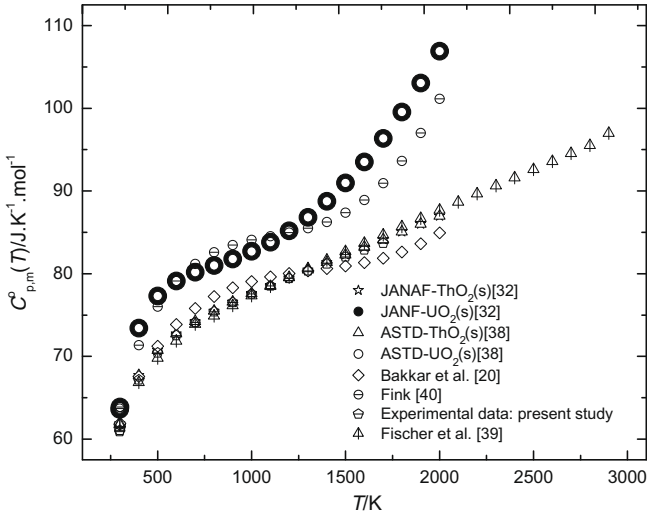

Fig. 4. A comparison of heat capacity data of $ThO_2(s)$ and $UO_2(s)$ reported in the literature. The heat capacity data for $ThO_2(s)$ obtained in this study is also compared.

highest temperature of measurement. Fig. 9 compares heat capacity data of $Th_{0.902}U_{0.098}O_2(s)$ by Springer et al. [6], Agarwal et al. [9], Kandan et al. [10], present study and additive oxide data. All studies show reasonable agreement. Fig. 10 shows comparison of heat capacity values of $Th_{0.8036}U_{0.1964}O_2(s)$ by Springer et al. [6], present study and additive oxide data. It also shows reasonable agreement among different studies.

The $C^{\circ}_{p,m}(T)$ values obtained in this study are combined with reasonably agreeing heat capacity values from the literature to obtain single expression for $ThO_2(s)$ and $Th_{1-y}U_yO_2(s)$ solid solutions. These expressions are given in Table 8.

The heat capacities of all compositions of solid solutions reported in the literature increases with increase in U/(Th + U) fraction. However, the heat capacities of $Th_{1-y}U_yO_2(s)$ ($y = 0.0392$, 0.0588) lie below those of both pure urania and thoria. After that the heat capacity values of the mixed oxide starts increasing with further addition of $UO_2(s)$. This trend is similar to the observation made by Fischer et al. [7] for transition temperature variation of the mixed oxides with change in composition of $UO_2(s)$. Hence heat capacity values of $Th_{1-y}U_yO_2(s)$ for $y = 0.02$, 0.1–0.9 obey additivity rule and it is less than additivity rule when y lies in between 0.02 and 0.08. Kandan et al. [10] have observed some of the $C^{\circ}_{p,m}(T)$ fit values of $Th_{0.1}U_{0.9}O_2(s)$ are slightly higher than those of $UO_2(s)$. This observation predicts that the heat capacities for mixed oxide solid solutions with U/(Th + U) fraction more than 0.9 are greater than that of pure $UO_2(s)$. If there is an error in fitting experimental data by Kandan et al. [10], this observation is incorrect. Thus, more heat capacity measurements with special attention for solid solutions with U/(Th + U) fraction more than 0.9 would be required to resolve it.

The heat capacities as a function of temperature and $UO_2(s)$ compositions have been computed using heat capacities of different compositions of mixed oxides given in Tables 8 and 14 and the computed expression is given as:

$$C^{\circ}_{p,m}\ (\mathrm{J\,K^{-1}\,mol^{-1}}) = 66.26 + 10.91\cdot y + (0.00923 - 0.00065\cdot y)\cdot(T/\mathrm{K}) - (6.7\cdot y + 7.70)\cdot 10^5\cdot(K/\mathrm{T})^2 \quad (0.019 \le y \le 0.9)\ \text{and}\ (298.15 \le T/\mathrm{K} \le 2000). \tag{22}$$

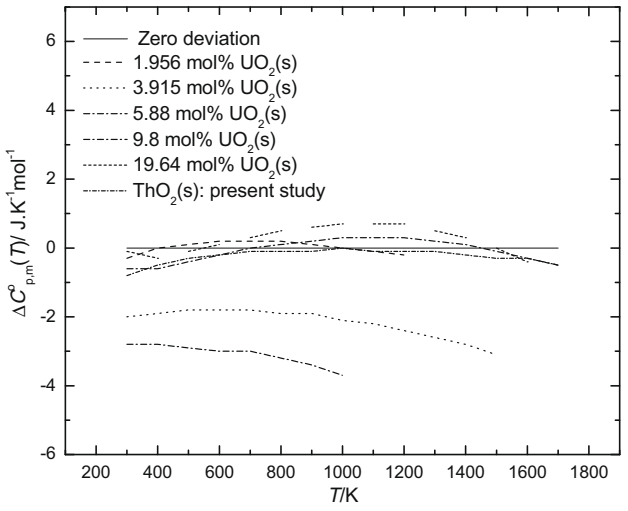

Fig. 5. A plot of heat capacity difference ($\Delta C^{\circ}_{p,m}(T)$) between $Th_{1-y}U_yO_2(s)$ and its component oxides as a function of temperature. The zero deviation line represents same heat capacity values for $Th_{1-y}U_yO_2(s)$ and $\{1 - y(ThO_2(s)) + yUO_2(s)\}$.

4.2. Simfuel

The heat capacity data on Simfuel of thoria–urania are limited [9] contrast to that of urania [42–45]. Agarwal et al. [9] have measured enthalpy increment of 20,000 MWD/ton burn-up $Th_{0.9804}U_{0.0196}O_2(s)$ fuel. The present authors have measured heat capacities of same composition fuel at 4 at% burn up. The Simfuel of different burn ups along with undoped fuel have been compared and observed a close agreement between doped and undoped solid solutions. This observation indicates that there is no anomalous increase in specific heat capacities of stoichiometric Simfuel with burn up.

4.3. Thermodynamic tables

The optimized heat capacity data were used to compute other thermodynamic functions such as heat capacity, entropy and free energy function $\{\Phi^{o}_{m}(T) = -[G^{o}_{m}(T) - H^{o}_{m}(298.15K)]/T\}$, enthalpy, Gibbs energy, Enthalpy of formation and Gibbs energy of formation of solid solutions. The $\Delta_f H^{\circ}_{m}(298.15\ K)$ values of the solid solutions required for computation of thermodynamic functions were obtained from pure urania and thoria by applying molar additivity rule assuming no enthalpy of mixing. The $S^{\circ}_{m}(298.15\ K)$ values of $Th_{1-y}U_yO_2(s)$ have been calculated by assuming ideal entropy of mixing. In this study, required thermodynamic functions for computation were taken from JANAF tables [32]. The Gibbs energy of mixing of the present and reported solid solutions has been calculated from the expression:

$$\begin{aligned}\Delta_{mix}G_m(Th_{1-y}U_yO_2, s, T) &= \{\Delta_f G^{\circ}_{m}(Th_{1-y}U_yO_2, s, T)\} - \{(1-y)\cdot\Delta_f G^{\circ}_{m}(ThO_2, s, T) \\ &\quad + y\Delta_f G^{\circ}_{m}(UO_2, s, T)\} + T\cdot R\{(1-y)\cdot\ln(1-y) + y\cdot\ln y\}. \quad (23)\end{aligned}$$

The calculated Gibbs energy of mixing of the mixed oxide solid solutions studied in this study and that reported in the literature are plotted against U/{Th + U} fraction in Fig. 11 at 1500 K. The excess Gibbs energy values are very small at 1500 K for all solid solutions. This might be due to stoichiometric solid solutions behaving ideally at 1500 K. The thermodynamic tables for $Th_{0.9804}U_{0.0196}O_2(s)$, $Th_{0.9608}U_{0.0392}O_2(s)$ $Th_{0.9412}U_{0.0588}O_2(s)$, $Th_{0.902}U_{0.098}O_2(s)$ and $Th_{0.8036}U_{0.1964}O_2(s)$ have been calculated in the temperature range 298.15–2000 K and are given in Tables 9–13, respectively.

4.4. Oxygen potential

Oxygen potentials of $Th_{1-y}U_yO_{2+x}(s)$ were retrieved from the literature and are given in Table 15. Recently Schram [21] has analyzed each data point with respect to the oxygen pressure $p(O_2)$, the non-stoichiometry x, the temperature T and the uranium concentration y in $Th_{1-y}U_yO_2(s)$. The mixed oxide solid solution is regarded as an ideal solid solution of $UO_2(s)$, $ThO_2(s)$ and a hypothetical compound $U_aO_b(s)$. In this assumption $ThO_2(s)$ is treated as an inert solvent that does not participate in any of chemical equilibrium describing oxygen potential. By measuring thermodynamic properties of compound $U_aO_b(s)$ in two oxygen pressure ranges, Schram [21] has given a general expression of oxygen potential as:

$$\Delta\bar{G}_m(O_2) = 2RTf(x,y) + \Delta_r H^{\circ} - T\Delta_r S^{\circ}$$

where

$$f(x,y) = \frac{1}{b-2a}\ln\frac{x\{b-2a+(1-a)x\}^{a-1}}{\{(b-2a)y - ax\}^{a}} \quad (24)$$

The values of $\Delta_r H^{\circ}$ and $\Delta_r S^{\circ}$ for two different oxygen potential ranges are given in Table 15.

In this study, the oxygen potentials of $Th_{1-y}U_yO_{2+x}(s)$ have been calculated for $y = 0.0196–0.2$ and $x = 0.002–0.02$ at $T/K = 1273$, 1373 and 1473 K from Eq. (24). These data along with oxygen potential data by Ugajin [16] and that calculated for stoichiometric oxides in this study have been least-squares fitted as a function of excess oxygen x, uranium concentration y and temperature T. The corresponding expression is given as:

$$\begin{aligned}\Delta\bar{G}_m(O_2)/kJ\ mol^{-1} &= 0.029592\cdot(T/K)\cdot\ln x + 0.003436 \\ &\quad\cdot(T/K)\cdot\ln(0.5619 - 0.1161\cdot x) \\ &\quad - 0.033028\cdot(T/K)\cdot\ln(0.5619\cdot y - 1.1161\cdot x) \\ &\quad - 348 + 0.1767\cdot(T/K) \\ &\quad (0.019 \le y \le 0.2),\ (0.0 \le x \le 0.024)\ \text{and} \\ &\quad (1000 \le T/K \le 1500). \quad (25)\end{aligned}$$

The oxygen potential of $Th_{1-y}U_yO_{2+x}(s)$ ($y = 0.0196$, 0.0392, 0.0588, 0.098, 0.1964) have been calculated from Eq. (25) and are plotted as a function of oxygen non-stoichiometry in Fig. 12. It shows that oxygen potential of mixed oxide solid solution increases systematically with increase in thorium content, temperature and x in $Th_{1-y}U_yO_{2+x}(s)$.

4.5. Vaporization of $Th_{1-y}U_yO_2(s)$

The vaporization of thoria–urania solid solutions reported in the literature is also summarized in Table 15. The total vapour pressure of the metal bearing species over single phase mixed oxide solid solution have been measured by means of transpiration technique by Aitken et al. [22] and Alexander [23]. The former group measured the partial pressure of $UO_3(g)$ in the temperature range 1473–1873 K by passing dry air as carrier gas over $Th_{1-y}U_yO_{2+x}(s)$ with $y = 0.063$, 0.2, 0.25, 0.5. Alexander [23] measured vapour pressure of $UO_2(g)$ over the stoichiometric $Th_{1-y}U_yO_2(s)$ solid solutions with $y = 0.08$ and 0.2 in the temperature range 2373–2773 K by passing Ar–H_2 as a carrier gas. Yamawaki et al. [24] have studied vaporization of $Th_{1-y}U_yO_{2+x}(s)$ using mass spectrometer, in the temperature range 2298–2465 K for $y = 0.1$, 0.2, 0.4, 1. The optimized experimental data reported in Tables 9–13 were used to compute the vaporization behaviour of $Th_{1-y}U_yO_2(s)$. The $UO_2(g)$ pressure of $Th_{0.8036}U_{0.1964}O_2(s)$, measured by Alexander [23] were extrapolated to 2300 K, is 6×10^{-5} kPa whereas our computation gives much higher value of 2×10^{-2} kPa which is reasonably agreeing with that value

Table 14
Coefficients of the fit equations of enthalpy increment and heat capacity data of $Th_{1-y}U_yO_2(s)$ solid solutions, reported in the literature.

Author/years	Wt% $UO_2(s)$	Solid solutions	Temp range (K)	Method	$H^\circ_m(T) - H^\circ_m(298.15\ K)/J\ mol^{-1} = A\cdot(T/K) + B\cdot(T/K)^2 + C\cdot(K/T) + D$					$C^\circ_{p,m}(T)/JK^{-1}\ mol^{-1} = a + b\cdot(T/K) + C(K/T)^2$			
					Datatypes	A	$B\times10^3$	$C\times10^{-5}$	$-D$	Datatypes	a	$b\times10^3$	$-c\times10^{-5}$
Springer et al. [6]	10.3	$Th_{0.899}U_{0.101}O_2(s)$	340–2271	DC	F	69.3	3.766	4.821	22652	E	69.3	7.532	4.821
1967	20.4	$Th_{0.7996}U_{0.2004}O_2(s)$	324–2270		F	71.02	3.67	6.188	23464	E	71.02	7.34	6.188
Fisher et al. [7]	8.167	$Th_{0.92}U_{0.08}O_2(s)$	2303–3302[a]	IDC		–	–	–	–	–	–	–	–
1981			2850–3300[a]		G	128.11	–	–	155710	E	128.11	–	–
			2303–2800[b]		F	59.53	7.287	3.225	19479	E	59.53	14.574	3.225
			2898–3302[b]		F	33.04.	16.25	20.915	18310	E	33.04	32.5	20.915
	15.288	$Th_{0.85}U_{0.15}O_2(s)$	2292–3401[a]	IDC		-	–	–	–	–	–	–	–
			2950–3401[a]		G	152.37	–	–	219310	E	152.37	–	–
			2292–2803[b]		F	64.67	6.444	60.648	21888	E	64.67	12.888	60.648
			2949–3401[b]		F	44.06	14.51	19.299	20899	E	44.06	29.02	19.299
	30.473	$Th_{0.7}U_{0.3}O_2(s)$	2312–3437[a]	IDC		–	–	–	–	–	–	–	–
			2900–3437[a]		G	131.85	–	–	148640	E	131.85	–	–
			2312–2897[b]		F	58.01	9.701	15.456	18678	E	58.01	19.402	15.456
			2897–3437[b]		F	46.23	13.969	10.24	18461	E	46.23	27.938	10.24
Anthonysamy et al. [8]	10.204	$Th_{0.9}U_{0.1}O_2(s)$	473–973	DC	G	71.923	3.4659	10.72	25347	E	71.932	6.9318	10.72
1997	50.561	$Th_{0.5}U_{0.5}O_2(s)$	473–973		G	74.249	3.5114	12.154	26526	E	74.249	7.0228	12.154
	90.2	$Th_{0.1}U_{0.9}O_2(s)$	473–973		G	72.344	6.7454	11.518	26032	E	72.344	13.491	11.518
Agarwal et al. [9]	2	$Th_{0.9804}U_{0.0196}O_2(s)$	376–981	CV	G	76.86	1.7974	18.885	29410	G	76.86	3.595	18.885
2005	4	$Th_{0.961}U_{0.039}O_2(s)$	376–914	CV	G	67.824	4.399	6.8452	22909	G	67.824	8.798	6.8452
	6	$Th_{0.941}U_{0.059}O_2(s)$	376–991	CV	G	78.814	−0.3042	18.977	29836	G	78.814	-0.608	18.977
	10	$Th_{0.902}U_{0.098}O_2(s)$	376–991	CV	G	78.358	0.2328	17.749	29336	G	78.358	0.4656	17.749
Kandan et al [10][a]	10.204	$Th_{0.9}U_{0.1}O_2(s)$	298–800	DSC		–	–	–	–	G	71.63	10.65	13.56
2009	50.561	$Th_{0.5}U_{0.5}O_2(s)$	486–1775	DC	G	77.554	1.548	16.763	28883	E	77.554	3.096	16.763
	90.2	$Th_{0.1}U_{0.9}O_2(s)$	298–800	DSC	G	–	–	–	–	G	73.47	11.48	14.23
			486–1758	DC	G	75.946	2.974	14.844	27886	E	75.946	5.948	14.844
			298–800	DSC		–	–	–	–	G	73.63	14.79	12.89
			479–1805	DC		74.927	4.548	12.516	26942	E	74.927	9.096	12.516

DC, drop calorimety, IDC= Inverse drop calorimeter; CV, calvet calorimetry, F, experimental data fitted in this study; E, derived from enthalpy increments data in this study; G, given in the literature.
[a] Reported temperature range.
[b] Fitted temperature range in this study.

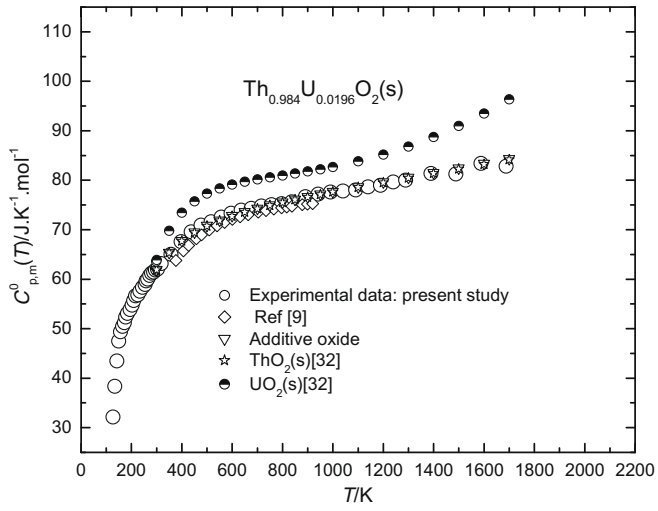

Fig. 6. A comparison of heat capacity data of $Th_{0.9804}U_{0.0196}O_2(s)$ of present study with those calculated from the literature.

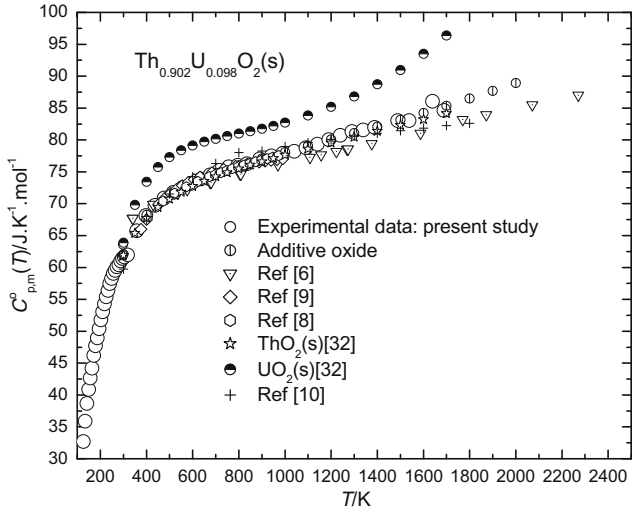

Fig. 9. A comparison of heat capacity data of $Th_{0.902}U_{0.098}O_2(s)$ of present study with those calculated from the literature.

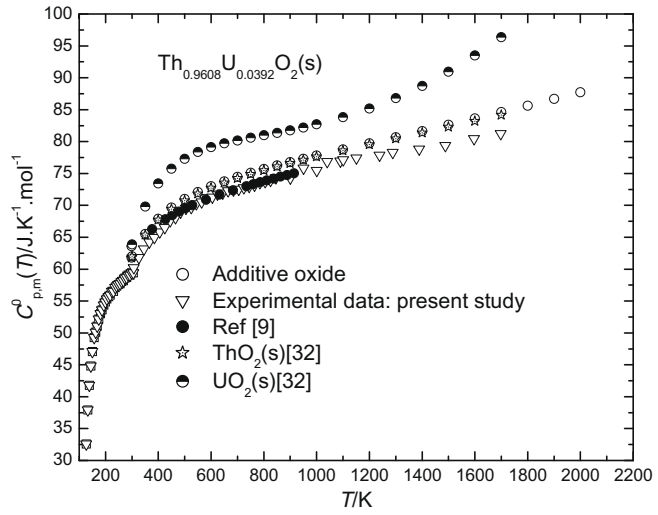

Fig. 7. A comparison of heat capacity data of $Th_{0.9608}U_{0.0392}O_2(s)$ of present study with those calculated from the literature.

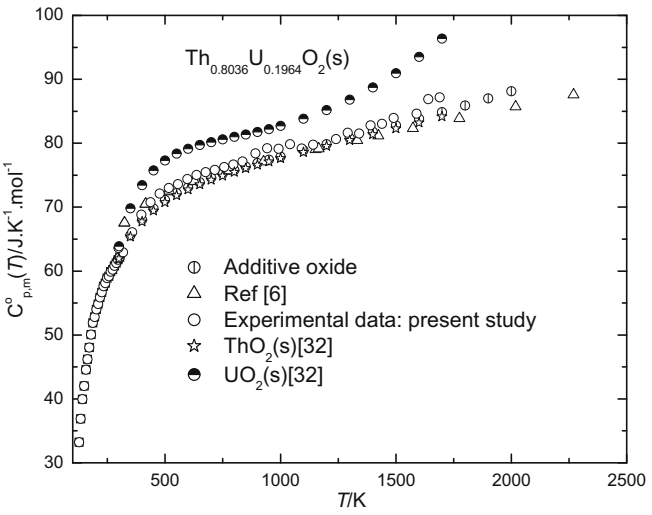

Fig. 10. A comparison of heat capacity data of $Th_{0.8036}U_{0.1964}O_2(s)$ of present study with those calculated from the literature.

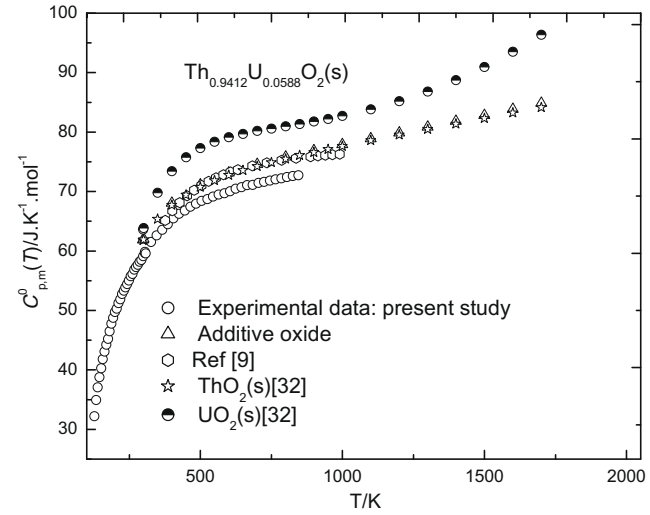

Fig. 8. A comparison of heat capacity data of $Th_{0.9412}U_{0.0588}O_2(s)$ of present study with those calculated from the literature.

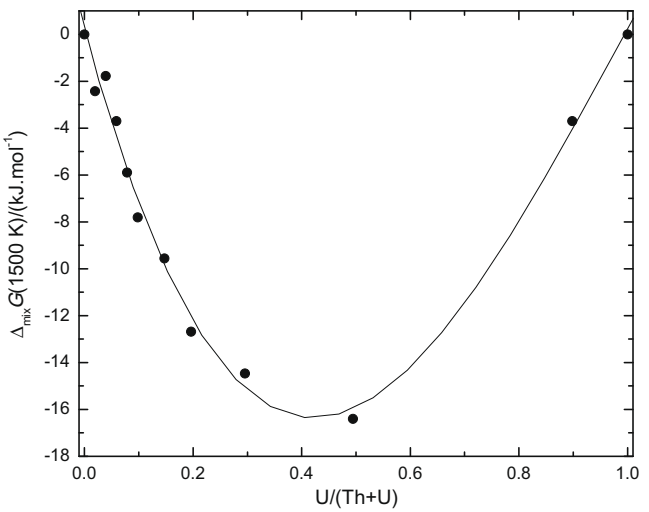

Fig. 11. The Gibbs energy of mixing of $Th_{1-y}U_yO_2(s)$ solid solutions as a function of U/(Th+U) fraction at 1500 K.

Table 15
Summary of reported oxygen potential measurements and vaporization studies on $Th_{1-y}U_yO_{2+x}$(s).

Authors	y range	T range	Method	Year
Oxygen potential measurements				
Anderson et al. [12]	0.03–0.244	1003–1203	Thermogravimetric analysis with gas volumetric method	1954
Roberts et al. [13]	0.0053–0.0597	1123	Pressure measurements	1958
Aronson and Clayton [14]	0.29–1	1250	Electromotive force measurements	1960
Tanaka et al. [15]	0.048–0.295	1250	Electromotive force measurements	1972
Ugajin et al. [16,17]	0.05–1	1273–1473	Thermogravimetric analysis	1982
Matsui and Naito [18]	0.2–1	1282–1373	Thermogravimetric analysis	1985
Anthonysamy et al. [19]	0.54–0.9	1073–1173	Electromotive force measurements	1997

Schram [21]	Computed			2005
	OP range	$\leqslant -100$ kJ mol^{-1}	>-100 kJ mol^{-1}	
	ΔH°_{m}	−426929	−114230	
	ΔS°_{m}	−226.95	−23.02	
	a	1.289	3.232	
	b	1.974	5.21	

Authors	y range	T range	Method	Atmosphere	Vapour species	Year
Vapour pressure measurements						
Aitkin [22]	0.063,0.2 0.25,0.5	1473–1873	Transpiration	Dry air	UO_3(g)	1966
Alexander et al. [23]	0.08, 0.2	2373–2773	Transpiration	Ar-H_2	UO_2(g)	1967
Ugajin et al. [17]	0.2	2000–2300	Estimated	–	UO_3(g)	1983
Yamawaki et al. [24]	0.1, 0.2, 0.4	2025–2192	Mass spectrometry	Vacuum	UO_2(g), UO_3(g)	1985

OP = oxygen potential.

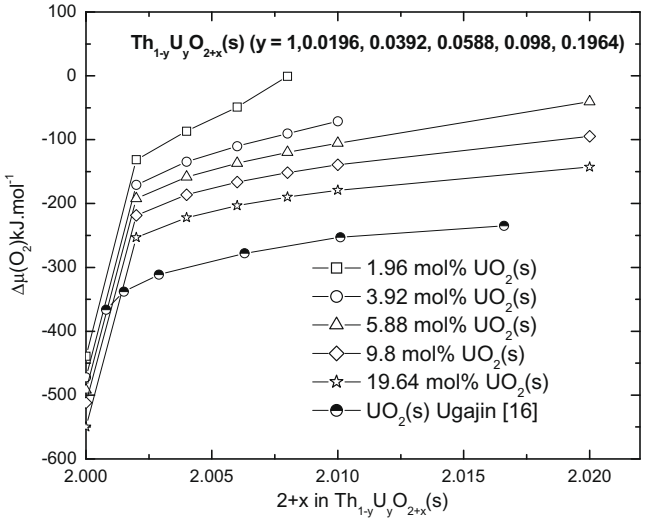

Fig. 12. The variation of oxygen potentials of $Th_{1-y}U_yO_{2+x}$(s) and UO_{2+x} as a function of oxygen nonstoichiometry, x at 1473 K.

(6×10^{-3} kPa) of Ugajin [17]. Thus, further experiments are needed to determine the pressures of gaseous actinide oxides over complete range of thoria–urania solid solutions. At fuel temperature in excess of 2300 K, the partial pressures of the oxides of the heavy metals are large enough to sustain fluxes of uranium and thorium through a gas phase contained in cracks or voids in the solid. The U/Th ratio of the vapour is not the same as the ratio of these species in the solid. In stoichiometric mixed oxides, UO_2(g), the dominant vapour species, is present in the gas phase in concentrations greater than ThO_2(g). In a temperature gradient, the UO_2(g) preferentially evaporate from the hot portion of this type of fuel and condenses in the cooler region, resulting in depletion of uranium in the solid at the hot zone.

Acknowledgements

The authors are grateful to Dr. A.K. Sengupta, Head, Fuel Properties Evaluation Section; Radiometallurgy Division for providing thoria-urania mixed oxide solid solutions for this study. The authors are also thankful to Dr. A. Goswami Head, Non Destructive Assay Section, Radiochemistry Division for least square analysis of data of three variables.

References

[1] K. Anantharaman, V. Shivakumar, D. Saha, J. Nucl. Mater. 383 (2008) 119.
[2] IAEA-TECDOC-1450, Thorium fuel cycle potential benefits and challenges, Vienna, 2005.
[3] R.K. Sinha, A. Kakodkar, Nucl. Eng. Des. 236 (2006) 683.
[4] P.G. Boczar, G.R. Dyck, J.D. Sullivan, R.J. Ellis, R.T. Jones, P. Taylor, A fresh look at thorium fuel cycles in CANDU reactors, in: Presented at IAEA Advisory Group Meeting on Thorium Fuel Cycle, Perspectives, 1997.
[5] IAEA-TECDOC-1496, Thermophysical Properties Database of Materials for Light Water Reactors and Heavy Water Reactors, Vienna, 2006.
[6] J.R. Springer, E.A. Eldridge, N.U. Goodyear, T.R. Wright, J.F. Lagedrox, BMI-X-10210, October 1967.
[7] D.F. Fischer, J.K. Fink, L. Leibowitz, J. Nucl. Mater. 118 (1983) 342.
[8] S. Anthonysamy, J. Joseph, P.R. Vasudeva Rao, J. Alloys Comp. 299 (2000) 112.
[9] R. Agarwal, R. Prasad, V. Venugopal, J. Nucl. Mater. 322 (2003) 98.
[10] R. Kandan, R. Babu, P. Manikandan, R. Venkata Krishnan, K. Nagarajan, J. Nucl. Mater. 384 (2009) 231.
[11] J. Ralph, J. Chem. Soc., Faraday Trans. 83 (1987) 1253.
[12] J. Anderson, D. Edgington, L. Roberts, E. Wait, J. Chem. Soc. (1954) 3324.
[13] L. Roberts, L. Russel, A. Adwick, A. Walter, M. Rand, in: Proc. Intern. Conf. Peaceful Uses of Atomic Energy, second, Geneva, vol. 28, 1958, p. 215.
[14] S. Aronson, J. Clayton, J. Chem. Phys. 32 (1960) 749.
[15] H. Tanaka, E. Kimura, A. Yamaguchi, J. Moriyama, J. Jpn. Inst. Metals 36 (1972) 633.
[16] M. Ugajin, J. Nucl. Mater. 110 (1982) 140.
[17] M. Ugajin, T. Shiratori, K. Shiba, J. Nucl. Mater. 116 (1983) 172.
[18] T. Matsui, K. Naito, J. Nucl. Mater. 132 (1985) 212.
[19] S. Anthonysamy, K. Nagarajan, P.V. Rao, J. Nucl. Mater. 247 (1997) 273.
[20] K. Bakker, E.H.P. Cordfunke, R.J.M. Konings, R.P.C. Scharm, J. Nucl. Mater. 250 (1997) 1.
[21] R.P.C. Schram, J. Nucl. Mater. 344 (2005) 223.
[22] E.A. Aitken, J.A. Edwards, R.A. Joseph, J. Phys. Chem. 70 (1966) 1084.
[23] C.A. Alexander, J.S. Ogden, G.W. Cunningham, Battelle Memorial Institute Report BMI-1789, 1967.
[24] M. Yamawaki, T. Nagasaki, M. Kanno, J. Nucl. Mater. 130 (1985) 207.
[25] M. Murabayashi, S. Namba, Y. Takahashi, T. Mukaibo, J. Nucl. Sci. Technol. 6 (1969) 128.
[26] Y. Takahashi, M. Murabayashi, J. Nucl. Sci. Technol. 12 (1975) 133.
[27] I.S. Kurina, L.S. Gudkov, V.N. Rumyantsev, Atomic Energy 92 (2002) 461.
[28] T.R.G. Kutty, R.V. Kulkarni, P. Sengupta, K.B. Khan, K. Bhanumurthy, A.K. Sengupta, J.P. Panakkal, Arun Kumar, H.S. Kamath, J. Nucl. Mater. 373 (2008) 309.
[29] J.P. Panakkal, H.S. Kamath, J. Nucl. Mater. 373 (2008) 309.
[30] G.K. White, F.W. Sheard, J. Low Temp. Phys. 14 (1974) 445.

[31] FactSage, Version 5.4.1, The integrated Thermodynamic Data Bank System, GTT-Technologies, GmbH, Germany, 1976–2006.
[32] S.C. Parida, S.K. Rakshit, S. Dash, S. Dash, V. Venugopal, J. Solid State Chem. 179 (2006) 2212.
[33] JANAF Thermochemical, Tables given in Database on Thermodynamic Properties of Individual Substances, Glushko Thermocentre, version 3.0, 1992–2000.
[34] C.H. Shomate, J. Phys. Chem. 58 (1954) 368.
[35] R. Paul, C. Keller, J. Nucl. Mater. 41 (1971) 133.
[36] H.J.C. Boekschoten, N.V. Kema, J. Inorg. Nucl. Chem. 30 (1968) 119.
[37] PCPDFWIN, JCPDS-ICDD, Version 2.2, Copyright 2001.
[38] O. Kubashewski, C.B. Alcock, P.J. Spencer, Materials Thermochemistry, sixth ed., Pergamon, Oxford, 1993.
[39] G.V. Belov, B.G. Trusov, ASTD Computer-aided Reference Book in Thermodynamical, Thermochemical, Thermophysical Properties of Species, Version 2, Moscov, 1983–1995.
[40] D.F. Fischer, L. Leibowitz, M.C. Chasanov, J. Nucl. Mater. 102 (1981) 220.
[41] J.K. Fink, J. Nucl. Mater. 279 (2000) 1.
[42] J.K. Fink, Int. J. Thermophys. 3 (1982) 165.
[43] P.G. Lucuta, H. Matzke, R.A. Verrall, H.A. Tasman, J. Nucl. Mater. 188 (1992) 198.
[44] R.A. Verrall, P.G. Lucuta, J. Nucl. Mater. 228 (1996) 251.
[45] H. Matzke, P.G. Lucuta, R.A. Verrall, J. Henderson, J. Nucl. Mater. 247 (1997) 121.